Passive Seismic Characterization of High Priority Salt Jugs in Hutchinson, Kansas: November 2021

Erik P. Knippel, Julian Ivanov, Shelby L. Peterie, Richard D. Miller,
Brett C. Bennett, Brett Wedel, Connor Umbrell, Olivia Jones, and Anthony Hoch

Kansas Geological Survey
1930 Constant Avenue
Lawrence, KS 66047

Report to

Stephen R. Hoffine
Burns & McDonnell
9400 Ward Parkway
Kansas City, MO 64114
816-839-9526

Open-file Report 2023-20 March 2022

The Kansas Geological Survey makes no warranty or representation, either express or implied, with regard to the data, documentation, or interpretations or decisions based on the use of this data including the quality, performance, merchantability, or fitness for a particular purpose. Under no circumstances shall the Kansas Geological Survey be liable for damages of any kind, including direct, indirect, special, incidental, punitive, or consequential damages in connection with or arising out of the existence, furnishing, failure to furnish, or use of or inability to use any of the database or documentation whether as a result of contract, negligence, strict liability, or otherwise. This study was conducted in complete compliance with ASTM Guide D7128-05. All data, interpretations, and opinions expressed or implied in this report and associated study are reasonably accurate and in accordance with generally accepted scientific standards.

Passive Seismic Characterization of High Priority Salt Jugs in Hutchinson, Kansas: November 2021

Executive Summary

This project appraised stress conditions of rock above selected dissolution voids by estimating the relative stress field from the calculated shear-wave velocity of the overburden. An estimate of change and the potential hazard each void represents can be obtained by comparing the current stress conditions with those measured on the previous survey. Shear-wave velocities were calculated using passive surface-wave methods. Data were acquired along thirteen profiles located on or near key abandoned brine production wells with train traffic used as an energy source. The multichannel analysis of surface waves (MASW) method provided an estimate of the shear-wave velocity, at a resolution sufficient to loosely map the alluvial/bedrock contact and velocity characteristics of the Permian-aged shale above the top of the "three finger" dolomite (at approximately 100 meters below ground surface). A key outcome was the differentiation of relative rock stress based on their shear velocity above salt jugs (associated with the target wells) compared to rocks above undisturbed salt or jugs without wide spans of unsupported roof rock. Comparisons of shear-wave velocity profiles over time (time lapse) provided insights into the consistency of overburden stability and, therefore indirectly, void dynamics.

Passive MASW data were continuously acquired above wells with a potential to impact surface access or assets over four nights (November 15-19, 2021) on the Vigindustries site in Hutchinson, Kansas. A continuous sampling approach targeting different wells each night was used to record all available train sources of passive source energy to maximize opportunities to capture energy with optimal source orientation and surface-wave characteristics. Surface waves were recorded with frequencies as low as approximately 4.5 hertz (Hz), representing an approximately 60 meter (m) average maximum depth of investigation, which generally represents a depth of more than 40 m below the bedrock surface.

Since shear modulus is the ratio of stress over strain and shear-wave velocity is a function of shear modulus and density, it is possible to estimate relative stress of overburden rocks (shear modulus) from shear-wave velocity values. Local increases in shear-wave velocity above background and without correlation to changes in lithology can be equated to increases in stress associated with changes in the distribution of overburden roof rock loading above dissolution jugs. Relative shear-wave velocity lows may be associated with remnants of a partial or incremental collapse whose vertical movement has been arrested by bulking or reduction in overburden stress due to redistribution within roof rock or changes in rock strength with vertical migration due to different geologic properties related to natural variation.

Overall shear-wave velocity directly over or in proximity to most of the 45 wells in this year's study is consistent with natural geologic conditions and a normal stress regime as observed on previous years' studies. Therefore, as in previous years (Morton et al., 2020a), the 2021 results suggest that the shale overburden is currently in a state of relative stability with localized changes suggesting future vertical migration might be possible at less than a dozen wells. Williams Street (line 9) is noted to have consistent velocity trends within the upper 30 m, but time-lapse variability deeper than 30 m over the past few years. This is possibly related to varying degrees of higher mode interference resulting from changes in stress conditions at depth related to changes in void characteristics. Overburden materials above seven wells from this November 2021 survey were interpreted to have subtle but notable changes in overburden characteristics relative to past years or expected for native conditions: 8A, 17, 42 (line 1), 14B (line 5), 19, 20, and 25 (line 15). Bedrock velocity at wells 2A and 4B, a major focus of past reports due to dynamic overburden conditions and possible limited failure at depth, has returned over the last year to an isotropic velocity condition as expected for currently stable environments at this site.

Introduction

Material properties (specifically stress accumulations) measured as a function of depth above abandoned salt jugs in Hutchinson, Kansas, appear related to the mobility and upward migration of load density associated with the tensional dome of these jugs. Localized escalation in stress (as indicated by increased shear-wave velocity) above subterranean voids is one indicator of an increased potential for roof failure and void migration (Eberhart-Phillips et al., 1989; Dvorkin et al., 1996; Khaksar et al., 1999; Sayers, 2004). Previous studies, using both active and passive seismic wavefield characteristics, suggest perturbations in the shear-wave velocity field immediately above voids can be correlated to characteristics of the unsupported roof spans of salt jugs in the Hutchinson area (Sloan et al., 2009; Sloan et al., 2010).

The strength of individual rock layers can be qualitatively described in terms of stiffness/ rigidity and empirically estimated from relative comparisons of shear-wave velocity measurements. Shear-wave velocity is directly proportional to stress and inversely related to non-elastic strain. Since the shear-wave velocity of earth materials changes when stress and any associated elastic strain on those materials becomes "large," it is reasonable to suggest load-bearing roof rock above mines or dissolution voids may experience elevated shear-wave velocities due to loading between pillars or, in the case of voids, loading between supporting side walls. This localized increase in shear velocity is not related to increased strength but to increased load as defined by Young's Modulus. High-velocity shear-wave "halos" encompassing low-velocity anomalies are suggested to be key indicators of near-term roof failure. All these phenomena have been observed within the overburden above voids in the Hutchinson Salt Member in Hutchinson at depths greater than 30 m below the bedrock surface.

Previous research projects at the Carey Boulevard Research Area (CBRA) correlated measured shear-wave velocities with the condition of dissolution void roofs and the physical properties of the overburden at selected locations on Vigindustries legacy solution mining property in Hutchinson. In 2008, active seismic reflection was used to evaluate the effectiveness of shear-wave velocity to estimate local stress above voids representative in the size and depth as those prevalent at the Vigindustries site. It was determined that the integrity of the overlying strata could be reasonably estimated using shear-wave seismic reflection imaging. The lack of necessary ultra-low-frequency surface waves in the recorded wavefield have negated attempts to use active-source multichannel analysis of surface waves (MASW) to estimate shear velocity in the lithified rocks above the voids and near the top of bedrock (Miller et al., 2009).

Uncontrolled local industrial and transportation activities represent sound sources that can produce the necessary low-frequency seismic waves to interrogated rock material at depths greater than 60 m using passive methods (Miller, 2011). Key to this method is the ability to estimate shear-wave velocities using MASW to depths more than double those possible using standard active sources (Park et al., 2004). Results of passive MASW studies at and near this site suggest that this method is effective in identifying jugs with heightened risk for upward migration (Miller, 2011; Ivanov et al., 2013).

Following the active seismic imaging study in 2008, two-dimensional (2-D) passive MASW surveys were acquired at the CBRA between 2012 and the present to appraise the stability of overburden at selected wells (Table 1) (Morton et al., 2020b, Morton et al., 2021). Results of these investigations suggested a normal stress regime with natural geologic variation in most wells. Shear velocity above a few wells was noted to be outside what might be considered normal for the area and justified more attention. Individually, each profile represents a snapshot in time. When combined with previous observations at the same locations, time-lapse

analysis can be used to monitor for temporal variation in shear velocity, providing insight into relative stability and void dynamics.

Table 1. Dates of and wells evaluated during 2-D passive MASW surveys at the CBRA.

Date	Wells
August 2012	2A, 1B, 2B, 3B, 5B, 6B, 7B, 12B
October 2012	2B, 4B, 6B, 17, 45, 52, 53, 59
March 2013	2A, 4B
November 2014	2A, 3B, 4B
March 2015	1B, 2B, 3B, 6B, 8A, 8B, 10B, 11B, 12B, 13B, 14B, 15B, 17, 18, 22A, 23, 23B, 29, 30, 39, 41, 42, 44, 45, 46, 86, 87, 88, 89, 90, 92
May 2015	2A, 4B
June 2015	4A, 6B, 7A, 7B, 52, 53, 59, 60
November 2017	2A, 4A, 7A, 8A, 1B, 2B, 3B, 4B, 6B, 7B, 8B, 10B, 11B, 12B, 13B, 14B, 15B, 17, 18, 22A, 23, 23B, 29, 30, 39, 41, 42, 44, 45, 46, 52, 53, 59, 60, 86, 87, 88, 89, 90, 92
October 2018	2A, 4B
December 2018	1B, 2B, 3B, 4A, 4B, 6B, 7A, 7B, 8A, 8B,10B, 11B, 12B, 13B, 14B, 15B, 17, 18, 22A, 23B, 23, 29, 30, 39, 41, 42, 44, 45, 46, 52, 53, 59, 60, 86, 87, 88, 89, 90
December 2019	1B, 2A, 2B, 3B, 4A, 4B, 5B, 6B, 7A, 7B, 8A, 8B, 10B, 11B, 12B, 13B, 14B, 15B, 17, 18, 22A, 23B, 23, 29, 30, 39, 42, 44, 45, 46, 52, 53, 59, 60, 88, 89, 90, 92
August 2020	2A, 4A, 7A, 15B, 59
November 2020	1B, 2A, 2B, 3B, 4A, 4B, 5B, 6B, 7A, 7B, 8A, 8B, 10B, 11B, 12B, 13B, 14B, 15B, 17, 18, 22A, 23B, 23, 29, 30, 39, 42, 44, 45, 46, 52, 53, 59, 60, 88, 89, 90, 92
November 2021	1B, 2A, 2B, 3B, 4A, 4B, 5B, 6B, 7A, 7B, 8A, 8B, 10B, 11B, 12B, 13B, 14B, 15B, 17, 18, 19, 20, 22A, 23B, 23, 25, 26, 29, 30, 33, 36, 39, 42, 44, 45, 46, 52, 53, 59, 60, 88, 89, 90, 92, 94

Geologic and Geophysical Setting

The Permian-aged Hutchinson Salt Member occurs in central Kansas, northwestern Oklahoma, and the northeastern portion of the Texas panhandle and is prone to and has an extensive history of dissolution and formation of sinkholes (Figure 1). In Kansas, the Hutchinson Salt Member possesses an average net thickness of 75 m and reaches a maximum of more than 150 m in the southern part of the basin. Deposition occurring during fluctuating sea levels caused numerous halite beds, 0.2 to 3 m thick, to be formed interbedded with shale, minor anhydrite, and dolomite/magnesite. Individual salt beds may be continuous for only a few miles despite the remarkable lateral continuity of the salt as a whole (Walters, 1978).

The distribution and stratigraphy of the salt is well documented (Dellwig, 1963; Holdoway, 1978; Kulstad, 1959; Merriam, 1963). The salt reaches a maximum thickness in central Oklahoma and thins to depositional edges on the north and west, erosional subcrop on the east, and facies changes on the south. The increasing thickness toward the center of the salt bed is due to a combination of increased salt and more and thicker interbedded anhydrites. The Stone Corral Formation (a well-documented seismic marker bed) overlies the salt throughout Kansas

(McGuire and Miller, 1989). Directly above the salt at this site is a thick sequence of Permian shale.

The upper 760 m of rock at this site is Permian shale (Merriam, 1963). The Chase Group (top at 300 m deep), lower Wellington Formation (top at 245 m deep), Hutchinson Salt (top at 120 m deep), upper Wellington Formation (top at 75 m deep), and Ninnescah Shale (top at 25 m deep) make up the packets of reflecting events easily identifiable and segregated within the Permian portion of the section (Figure 2). Bedrock is defined as the top of the Ninnescah Shale with the unconsolidated Pliocene-Pleistocene Equus beds making up the majority of the upper 30 m of sediment. The thickness of Quaternary alluvium that fills the stream valleys and paleosubsidence features ranges from 0 to as much as 90 m, depending on the dimensions of the features.

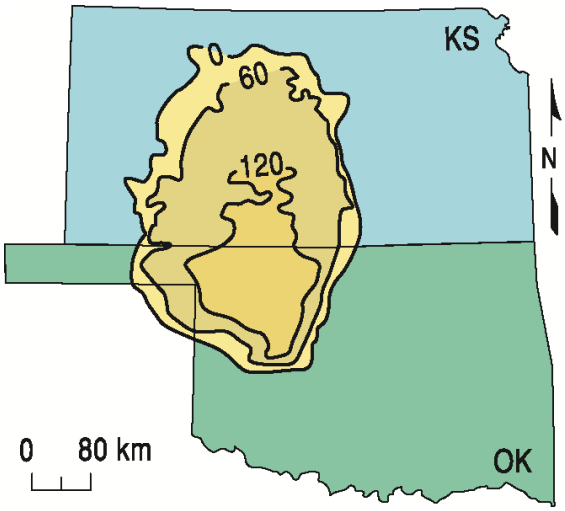

Figure 1. Approximate extent of salt formation, with contour intervals expressed in meters.

Recent dissolution of the salt and resulting subsidence of overlying sediments forming sinkholes has generally been associated with mining or saltwater disposal (Walters, 1978). Historically, these sinkholes can manifest themselves as a risk to surface infrastructure. The rate of surface subsidence can range from gradual to very rapid. Besides risks to surface structures, subsidence features potentially jeopardize the natural segregation of groundwater aquifers, greatly increasing their potential to negatively impact the environment (Whittemore, 1989, 1990). Natural sinkholes resulting from dissolution of the salt by localized leaching within natural flow systems that have been altered by structural features (such as faults and fractures) are not uncommon west of the main dissolution edge (Merriam and Mann, 1957).

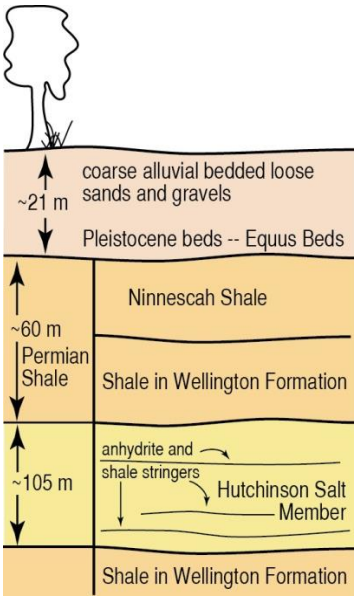

Figure 2. Generalized geology.

Caprock and its characteristics are a very important component of any discussion concerning dissolution, subsidence, and formation of sinkholes. The Permian shales (Wellington and Ninnescah) that overlay the Hutchinson Salt Member are about 60 m thick in this area and are characterized as generally unstable when exposed to freshwater, being susceptible to sloughing and collapse (Swineford, 1955). These Permian shales tend to be red or reddish-brown and are commonly referred to as “red beds.” Permian red beds are extremely impermeable to water and have provided an excellent seal between the freshwaters of the Equus beds and the extremely water-soluble Hutchinson Salt Member. The modern-day expanse and mere presence of the Hutchinson Salt is due to the protection from freshwater provided by these red beds.

Isolating the basal contact of the Wellington Formation provides key insights into the general strength of roof rock expected, if dissolution-mined salt jugs (salt jugs are the jug-shaped

cavities or voids in the salt that form after salt has been dissolution mined in proximity to the wells) reach the top of the salt zone. Directly above the salt/shale contact is an approximately 6 m thick dark-colored shale with joint and bedding cracks filled with red halite (Walters, 1978). Once unsaturated brine comes in contact with this shale layer, these red halite-filled joints and bedding planes are rapidly leached, leaving an extremely structurally weak layer.

Field Layout and Data Acquisition

To ensure the highest quality (e.g., signal to noise ratio) data and maximum crew safety, receivers were deployed during daylight hours and train data were recorded at night when cultural and industrial noise was minimal, thereby providing the highest possible signal-to-noise ratio. Analysis of previous seismic energy sources captured during passive recording at this site clearly indicated trains at distances of 2 kilometers (km) or more provided the best broad spectrum, low-frequency seismic energy (Miller, 2011). Since seismic energy with characteristics best suited for this study may arrive when trains are at distances greater than can be detected by spotters, seismic energy was recorded continuously throughout the night to ensure the capture of all times possessing optimum data.

Data were acquired November 15-18, 2021. A total of thirteen seismic lines (Figure 3) were deployed during the day over this four-day period. Line layout was designed to cross directly over all wells of interest. A 2-D square grid of receivers was recorded simultaneously to allow determination of the incident orientation of passive seismic energy. Seismic receivers were single ION 4.5 Hz geophones spaced at 3 m intervals. The seismic lines collectively totaled approximately 5000 m in length. The 2-D monitoring/alignment grid consisted of 131 receivers spaced at 5 m intervals and was configured to form four concentric expanding squares with 10, 30, 50, and 70 m sides (Figure 4). Data were recorded with a 400+ channel 24-bit Geometrics Geode distributed seismic system. Line 15 and the 2-D grid utilized a wireless nodal acquisition system by GTI that recorded output from the geophones. Seismic records from the Geometrics system were 30 seconds (s) long with a 2 millisecond (ms) sampling interval. In total, 3259 seismic records were recorded.

Processing and Analysis

Data were processed using algorithms developed at the Kansas Geological Survey (KGS). The passive method used for this study is well published and has consistently proven effective, producing good-quality results on other studies (Park et al., 2004; Ivanov et al., 2013). The continuous-data-acquisition method records energy from nearby sources at various orientations with respect to the seismic line. Data from the 2-D grid are evaluated for optimized source alignment with respect to each 1-D seismic line allowing data rotation and analysis or direct analysis of only data from near in-line sources.

For each line, the surface-wave amplitudes recorded by the 2-D grid were plotted as phase velocity versus frequency across a range of azimuths (0 to 360 degrees) (Figure 5), relative to the seismic line. This display was effective for identifying the best broad-band, low-frequency source energy with an azimuth as near zero as possible. Seismograms for each line were selected and segmented into the shortest groups of receivers (“spread length”) with optimum source

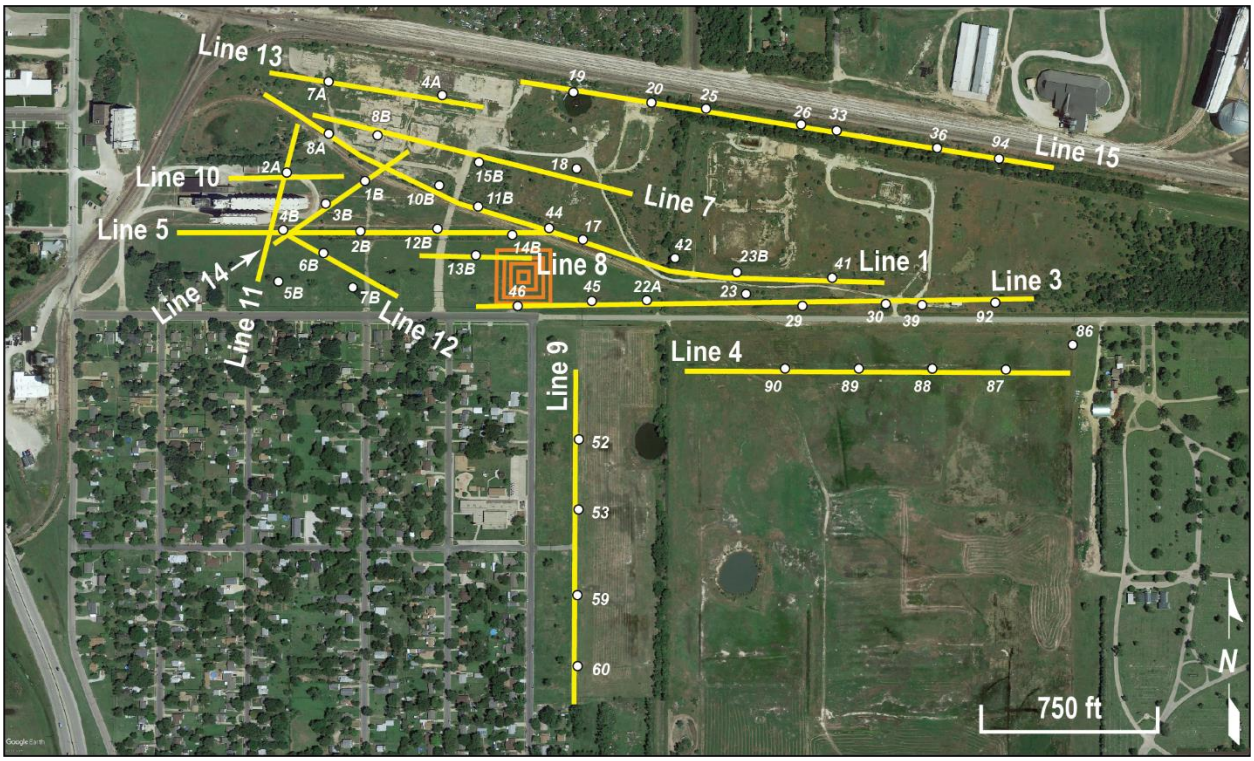

Figure 3. Aerial photo with GPS locations of thirteen seismic lines, 2-D grid of receivers (orange squares), and wells in the November 2021 study.

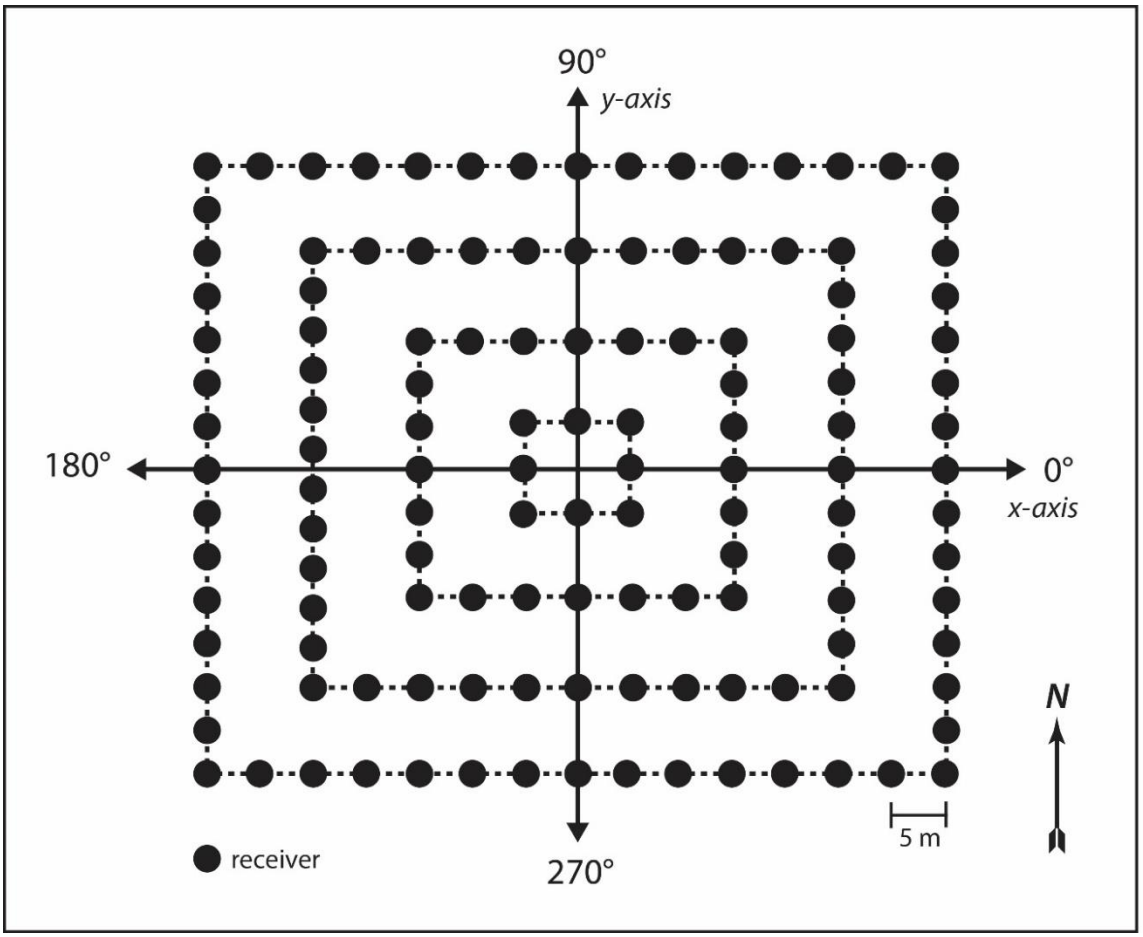

Figure 4. Four nested square arrays were deployed each night to construct the 2-D square grid for determining incident source azimuth information.

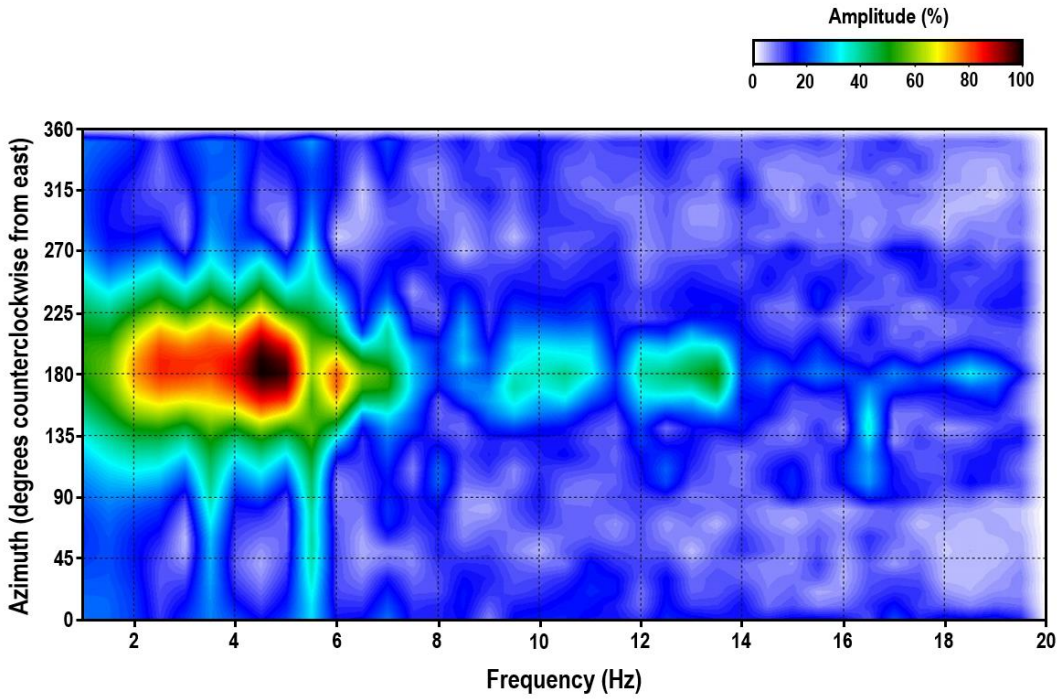

Figure 5. Azimuth plot indicating the direction of the dominant passive source energy (in degrees counter-clockwise from east). Here, the dominant passive source energy is centered on approximately 180°.

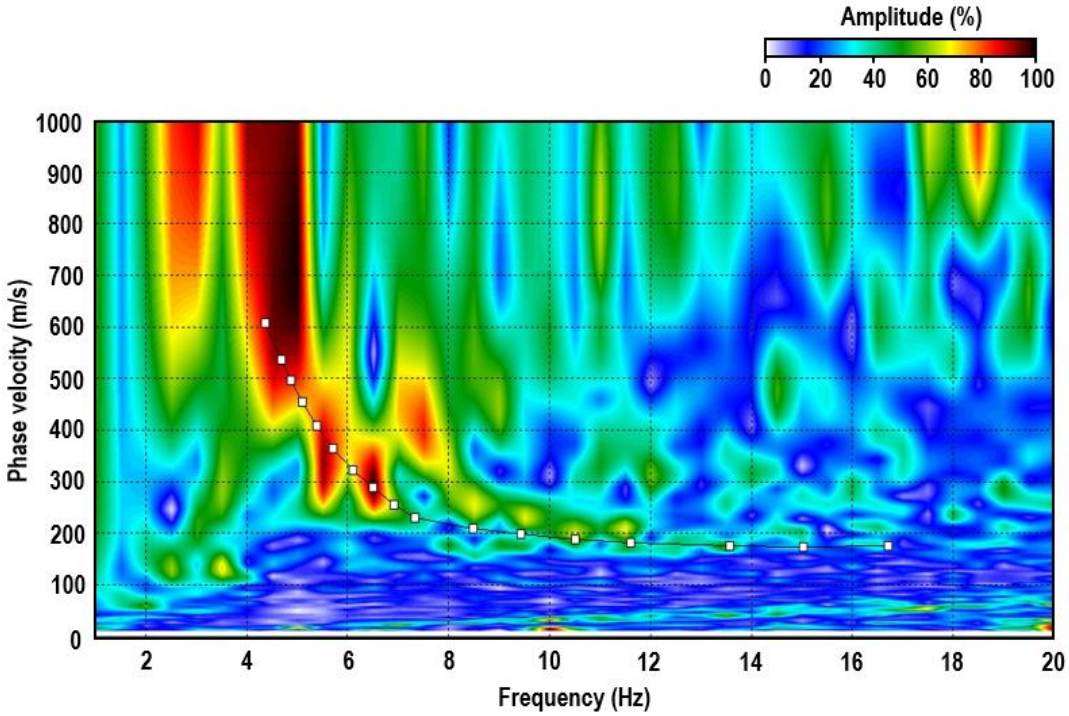

Figure 6. Dispersion pattern with high signal-to-noise ratio of the fundamental-mode Rayleigh wave.

characteristics that resulted in dispersion patterns on phase velocity versus frequency plots with the greatest percentage of high-amplitude fundamental-mode Rayleigh-wave energy and minimal higher-order surface-wave interference (Figure 7).

Fundamental-mode dispersion curves were picked and inverted to obtain a 2-D section of shear-wave velocity as a function of depth. The apparent velocity (v_{app}) is:

$$v_{app} = \frac{v_{act}}{(\cos\theta)} \tag{1}$$

where v_{act} is the actual seismic velocity and θ is the azimuth of the source with respect to the seismic line determined from the azimuth versus frequency plot. Thus, the percent increase in velocity (Δv) is:

$$\Delta v = \frac{1}{\cos\theta} - 1 \tag{2}$$

Equation 2 was used to calculate the increase in velocity due to the source azimuth for each line (Table 2).

Table 2. Directions of the passive seismic sources and the seismic lines; spread length used for processing, the angle of the source with respect to the line (θ, in degrees counterclockwise from east), and the percent increase in apparent velocity (Δv) attributable to oblique source orientations.

	processing spread length(s)	source orientation	line orientation	θ	Δv
Line 1	57 m 57 m	120° 180°	135° 180°	15° 0°	3.53% 0%
Line 3	57 m	180°	180°	0°	0%
Line 4	57 m	180°	180°	0°	0%
Line 5	57 m	180°	180°	2°	0.06%
Line 7	57 m	180°	165°	15°	3.53%
Line 8	57 m	180°	180°	0°	0%
Line 9	57 m	90°	86°	4°	0.24%
Line 10	57 m	180°	180°	0°	0%
Line 11	57 m	90°	74°	16°	4.03%
Line 12	57 m	150°	152°	2°	0.06%
Line 13	57 m	165°	172°	7°	0.75%
Line 14	57 m	45°	35°	10°	1.54%
Line 15	57 m	180°	165°	15°	3.53%

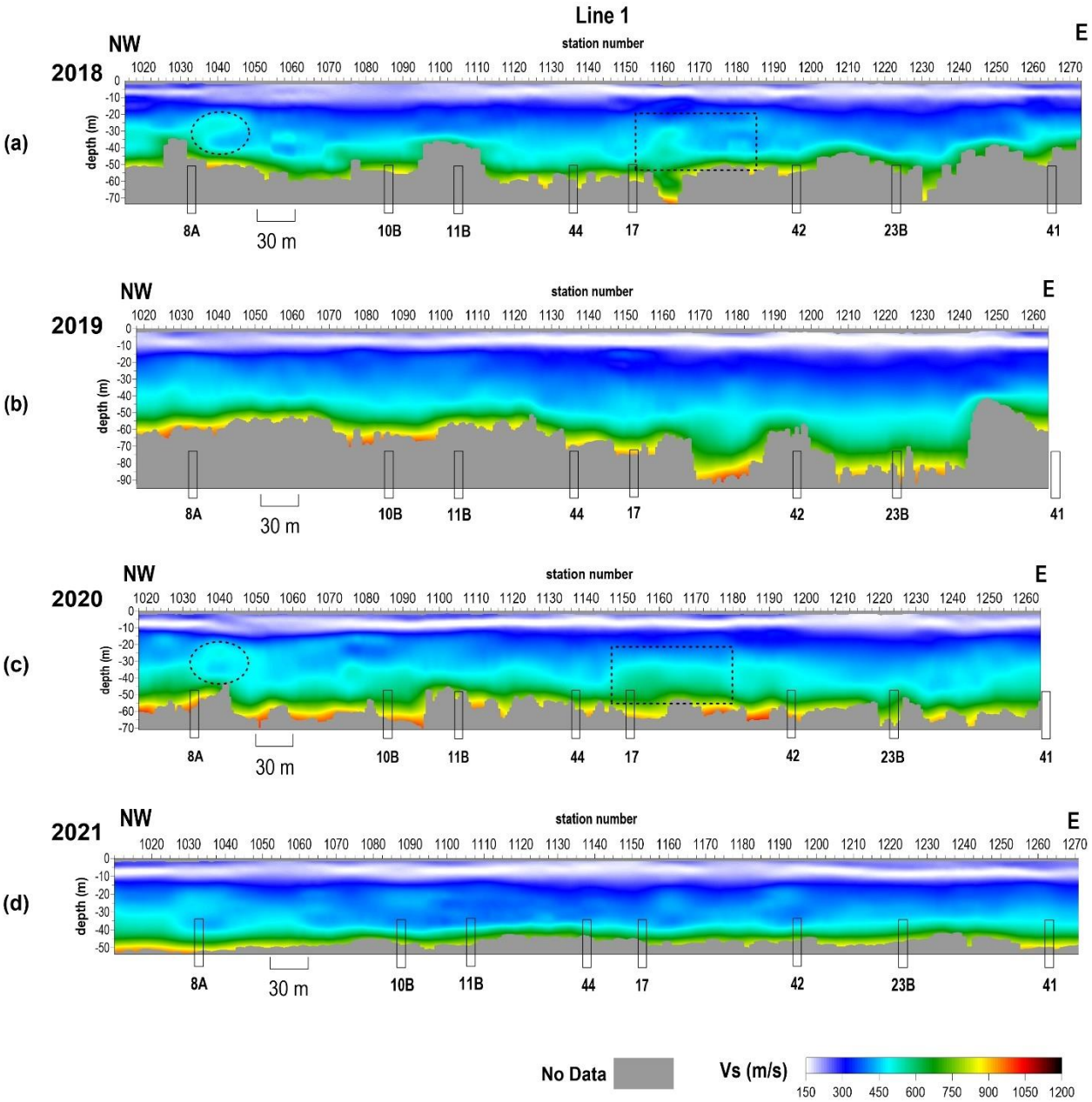

Figure 7. Shear-wave velocity profiles from line 1 from (a) December 2018, (b) December 2019, (c) November 2020, and (d) November 2021.

Field Results and Observations

General Trends

The average velocity of the upper 15 m is approximately 175 m/s, consistent with the unconsolidated/alluvial sediment expected in this area. The velocity gradient at 15 m coincides with the interface between the unconsolidated sediment and shale bedrock. Average depth of investigation was 50-55 m across all lines, as fundamental-mode energy was attenuated for frequencies lower than 4 Hz over much of the data. Dispersion curves for each line were created by stacking overtone images from multiple source records. This technique improves the quality and coherency of the fundamental mode across low frequencies. Sufficient and representative fundamental-mode dispersion curves were obtained using shorter spread lengths than previous years. Shorter spreads increased both the lateral resolution and spatial extent of the resulting 2-D profiles (allowing for Vs assessment over wells previously beyond the 2-D profiles in previous years) while maintaining depths of investigation well below top of bedrock (40 m or deeper across all stations).

Line 1

Line 1 (Figure 7) is a slightly curved NW-E oriented line that extends across wells 8A, 10B, 11B, 44, 17, 42, 23B, and 41 (Table 3). Large spread lengths in previous years limited the 2-D profile to west of well 41; shorter spread length used for processing this year extended the profile to allow assessment of Vs around well 41. Line 1 is the only line in this deployment with a nonlinear receiver alignment. Two different source files were used to process the line, one with an azimuth of 120 degrees and the other with 180 degrees. The two overtone images were combined and assigned a relative prominence over the other based on the station location. Combining data in this manner produces a smooth transition between sources across the line as opposed to stitching results from independently processed subsets. The depth of investigation was between 50 and 60 m, which is consistent with last year's study. Variations in overtone image amplitudes were observed on this line in as few as 30 stations (Figure 8). The overtone image for station 1103 has strong fundamental-mode energy between 3.5 Hz and 7 Hz with some multimode behavior. At station 1132, however, the strongest energy is observed below 4 Hz with a fundamental mode at higher frequencies still present. However, the dispersion curve trends are similar, and therefore the velocity profile is as well.

Table 3. Wells and corresponding station numbers across line 1.

Well	8A	10B	11B	44	17	42	23B	41
Station No.	1033	1086	1105	1136.5	1152.5	1196	1223.5	1265

Overall, the bulk velocity trend observed in November 2021 is generally consistent with the past three years' results. A halo anomaly over well 8A observed in 2018 and 2020 (dashed circle in Figure 7a,c) remains relatively unchanged in 2021 (Figure 7d). An area of slightly elevated velocity was observed east of well 17, where an area of increased velocity was observed in 2020. Overall velocity trend is more consistent with the 2019 result that shows a more uniform profile between wells 17 and 42 with subtle velocity halos near these wells. The velocity variation across line 1 is relatively minimal and all identified anomalies are within the bounds of native material.

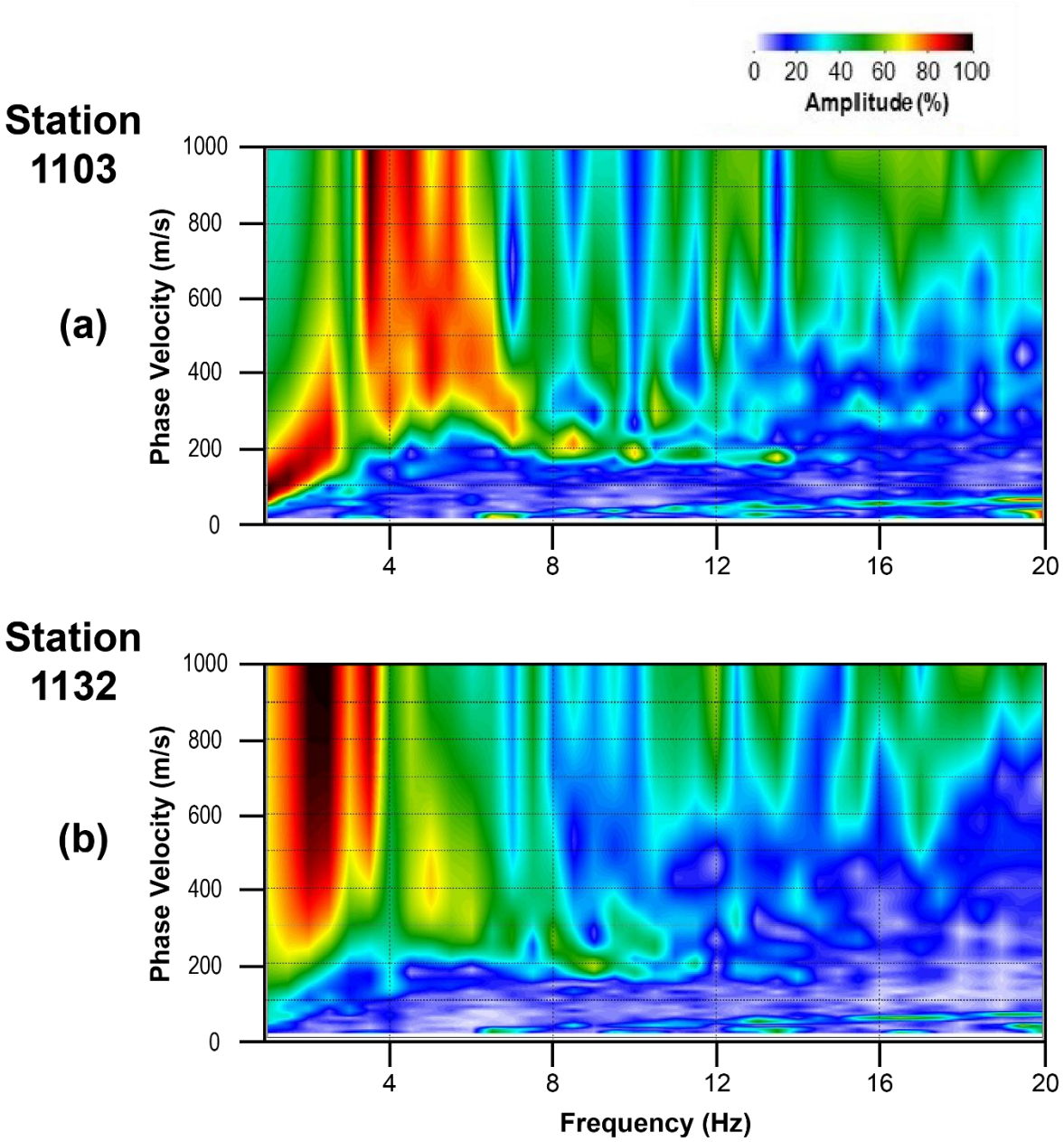

Figure 8. Changes in dispersion curve amplitude and coherency along line 1.

Line 3

Line 3 (Figure 9) is oriented W-E and extends over wells 46, 45, 22A, 23, 29, 30, 39, and 92 (Table 4). The general bulk velocity profile remains consistent with past studies. Intermittent velocity inversions were observed in the 2021 data towards the western extent of the line between wells 46 and 45 and east of 22A. Possible halo anomalies were identified around well 45 in 2018 and 22A in 2020 (Figure 9a,c). Dispersion curves between these two wells had limited low-frequency fundamental-mode energy in 2019, and the average depth of investigation was limited to about 30 m. The velocity of the upper 40-50 m in the 2021 data are consistent across the line and consistent with the range expected for native material. An area of slightly elevated velocity between wells 39 and 92 (stations 3200 and 3230) was also present in past years.

Table 4. Wells and corresponding station numbers across line 3.

Well	46	45	22A	23	29	30	39	92
Station No.	3025	3057	3080.5	3124	3148	3183.5	3199	3230.5

Line 4

Line 4 is a W-E oriented line that crosses wells 90, 89, 88, and 87 at stations 4044, 4076, 4107.5, and 4139.5, respectively (Figure 10). The bulk velocity trend for 2021 is consistent with past years and laterally consistent across the line. Anomalous velocity profiles observed between stations 4050 and 4055 in 2018 and 2020, respectfully, are not observed in 2021 data. Shorter spread lengths this year allowed imaging of the subsurface on both sides of well 87. The velocity profile on the east side of well 87 is consistent with the rest of the line. The bulk velocity profile supports normal geologic conditions.

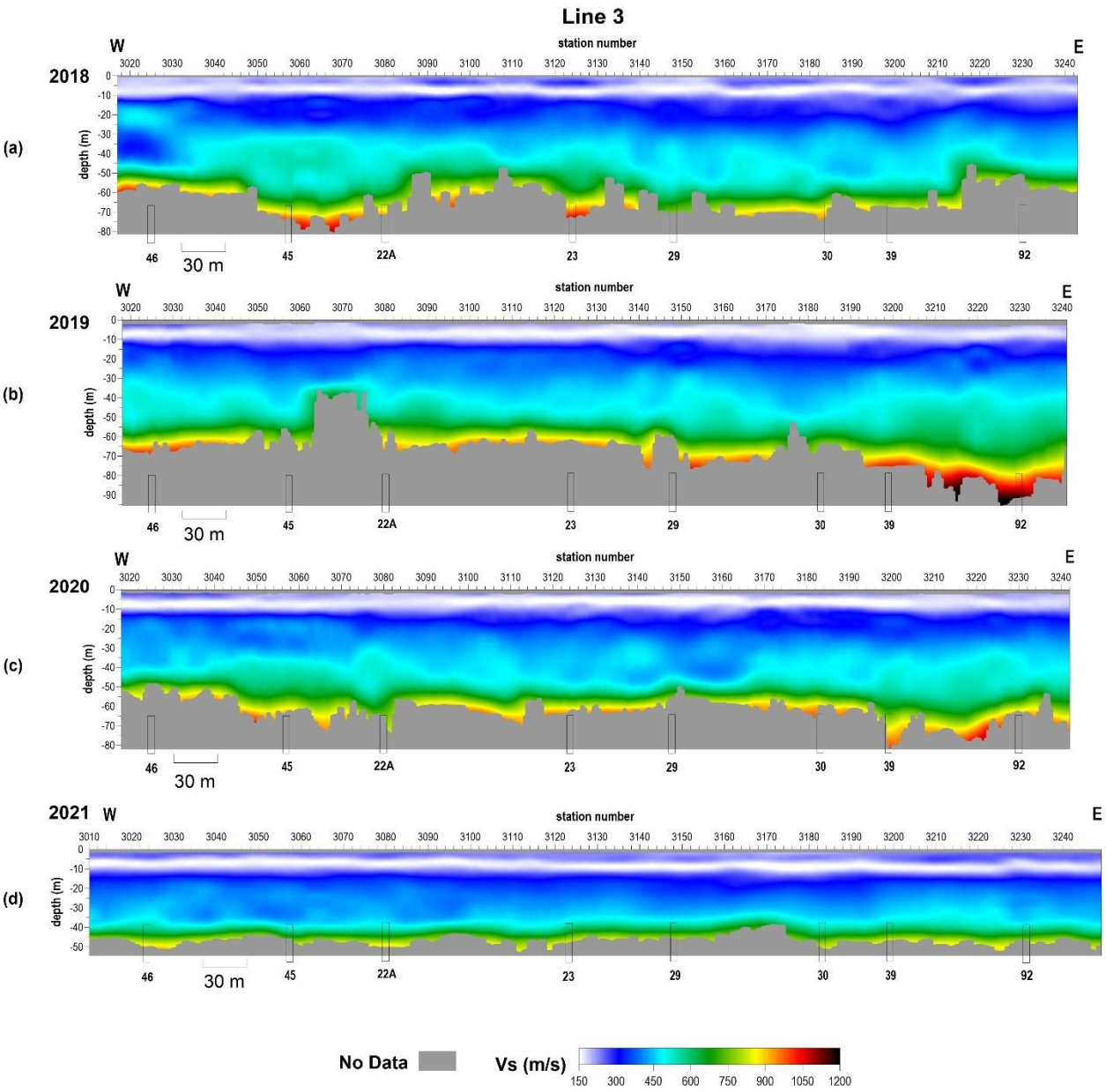

Figure 9. Shear-wave velocity profiles from line 3 from (a) December 2018, (b) December 2019, (c) November 2020, and (d) November 2021.

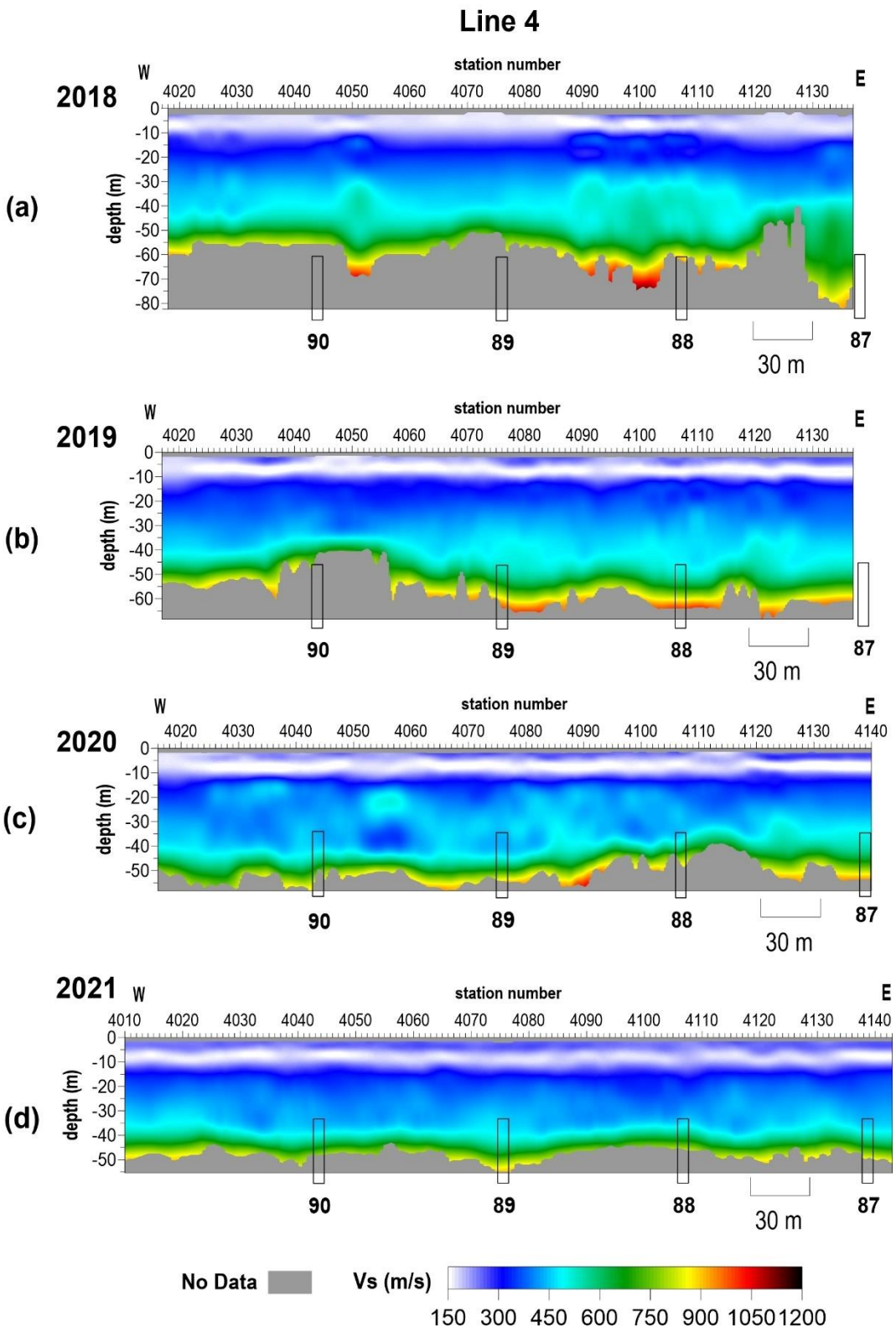

Figure 10. Shear-wave velocity profiles from line 4 from (a) December 2018, (b) December 2019, (c) November 2020, and (d) November 2021.

Line 5

Line 5 is oriented W-E and crosses wells 4B, 2B, 12B, and 14B at stations 5027.5, 5061, 5094, and 5126.5, respectively (Figure 11). A dome-shaped area of elevated velocity is observed near well 14B. Anomalous velocity trends have consistently been observed near this well in previous years. The dome-shaped anomaly between wells 2B and 12B and associated presence of higher modes in 2020 is absent in 2021 (Figure 12).

Line 7

Line 7 is oriented NW-SE and crosses over wells 8B, 15B, and 18 approximately located at stations 7028, 7073, and 7114, respectively (Figure 13). Overall bulk velocity remains relatively consistent across the line compared to previous studies and is consistent with the native material. Although the depth of investigation was slightly reduced compared to previous years, the upper 40-50 m is fairly consistent. Elevated velocity at depth and associated increase in depth of investigation near well 15B prompted a midyear monitoring survey in August 2020. Time-lapse observations from 2019 to 2021 (Figure 14) suggest dynamic changes at this well, and conditions currently appear to be stable.

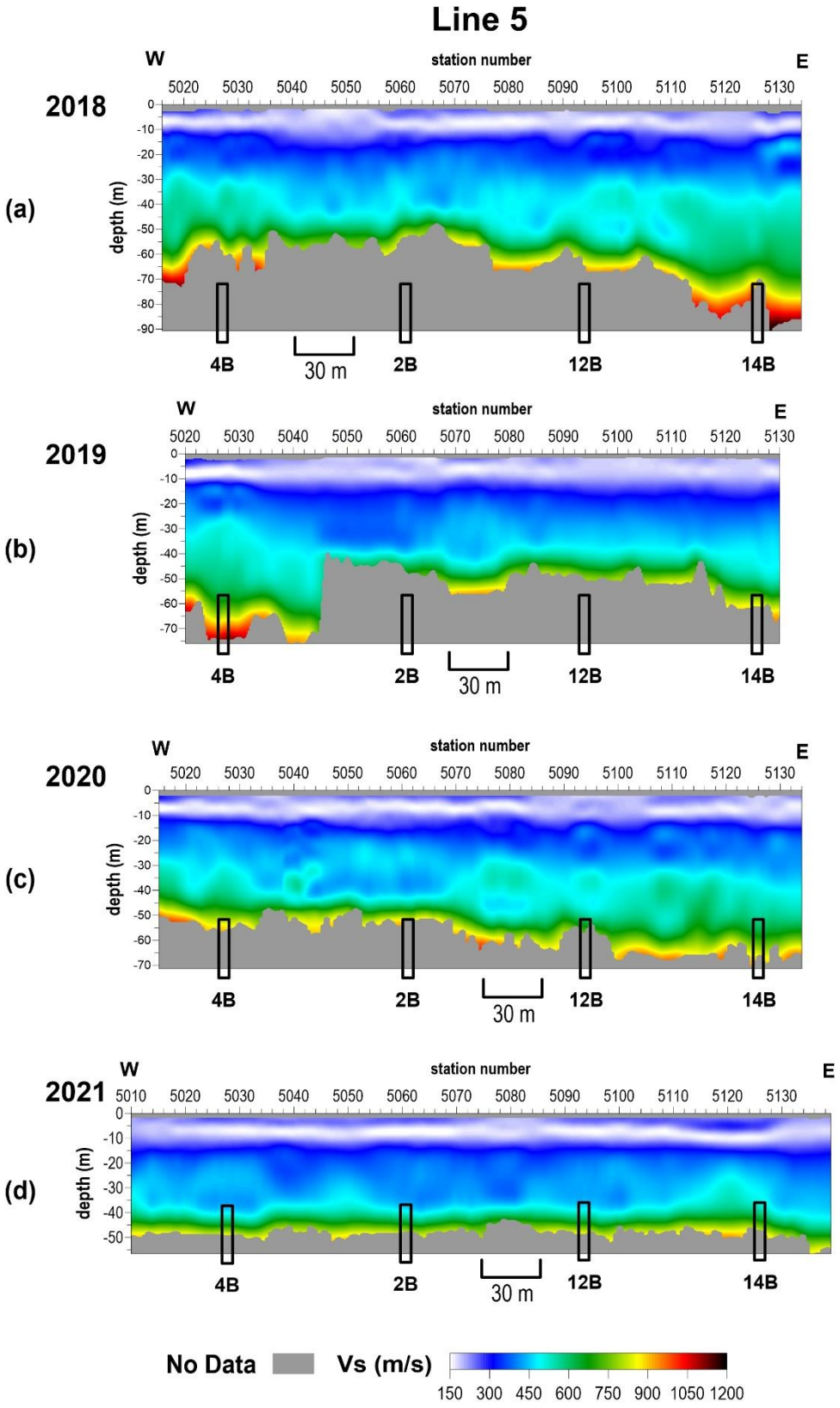

Figure 11. Shear-wave velocity profiles from line 5 from (a) December 2018, (b) December 2019, (c) November 2020, and (d) November 2021.

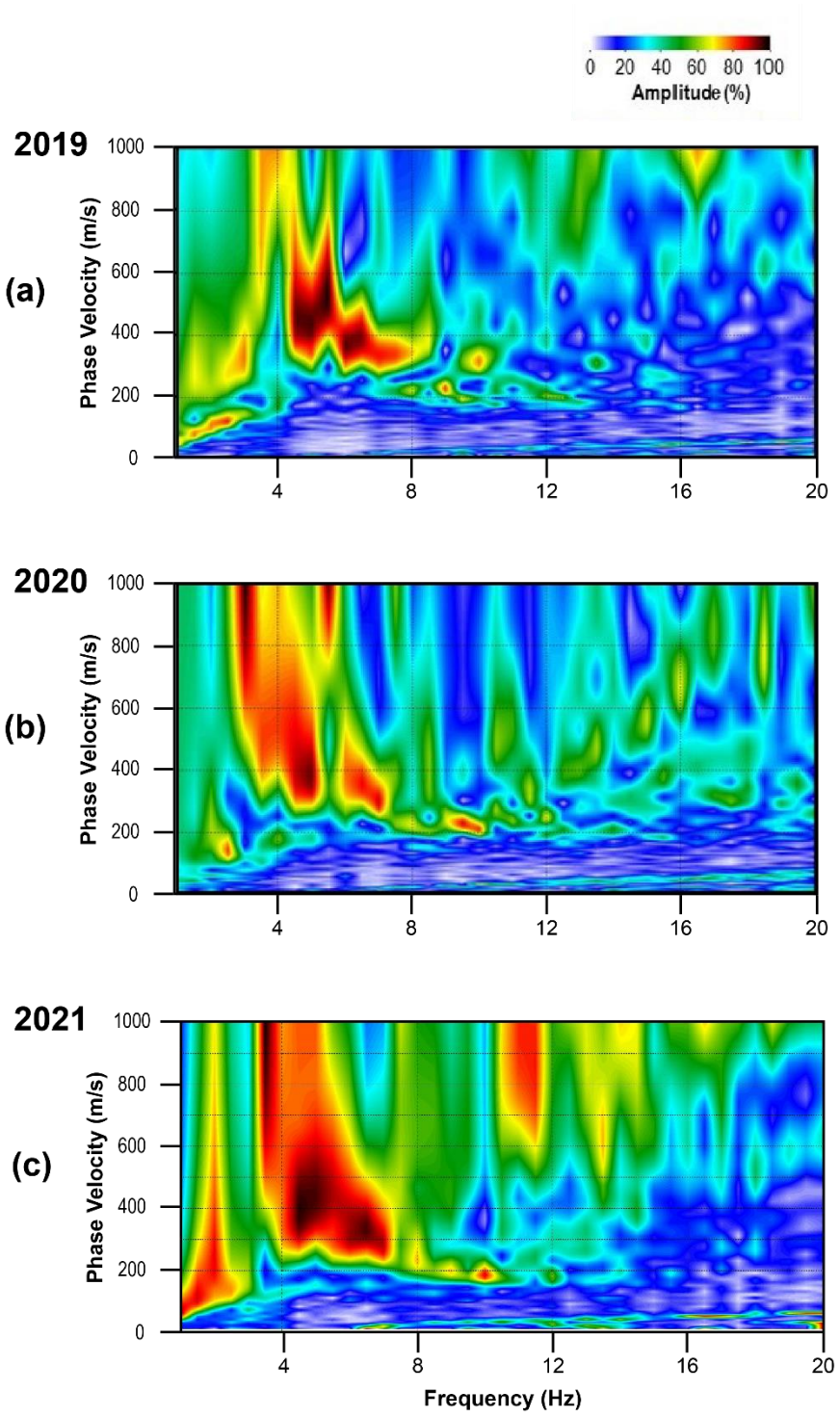

Figure 12. Representative dispersion curves from (a) 2019, (b) 2020, and (c) 2021 with varying levels of signal quality across line 5.

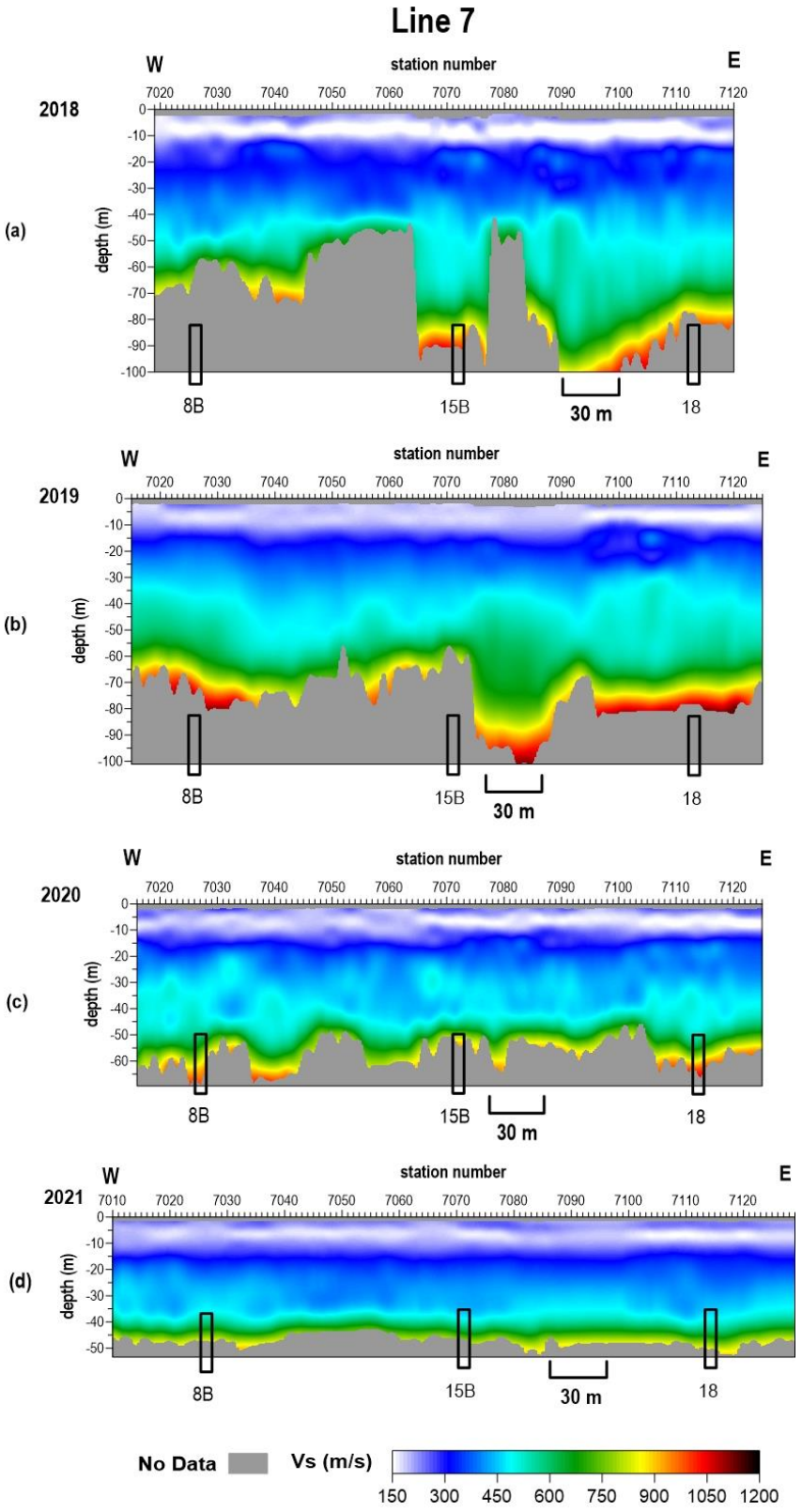

Figure 13. Shear-wave velocity profiles from line 7 from (a) December 2018, (b) December 2019, (c) November 2020, and (d) November 2021.

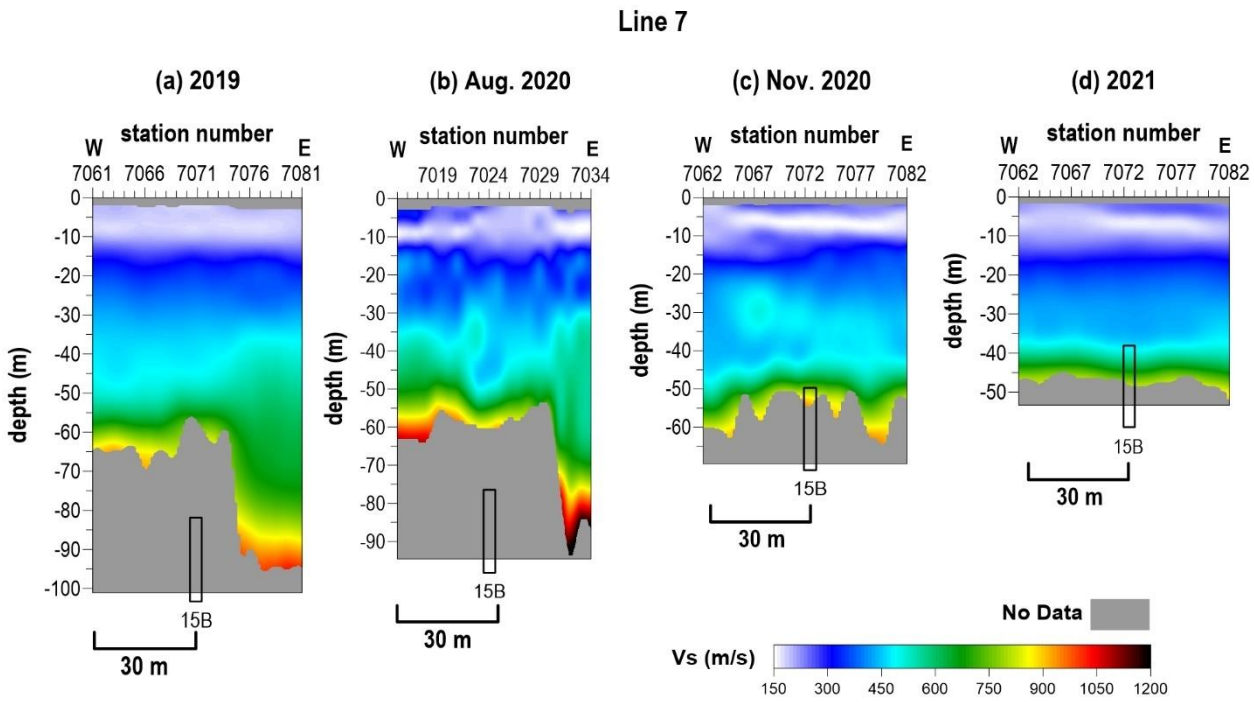

Figure 14. Shear-wave velocity profiles from the area surrounding well 15B on line 7 from (a) December 2019, (b) August 2020, (c) November 2020, and (d) November 2021.

Line 8

Line 8 is oriented W-E and intersects well 13B at station 8025 (Figure 15). The four westernmost stations on line 8 extend across the paved entry road at the CBRA; these four stations (8008-8011) required rock plates rather than steel spikes to couple sensors to the ground surface. The bulk velocity profile in 2021 is consistent with the past two years' results. Dynamic velocities have been observed at well 13B in the past few years. Velocity was elevated in 2018 and returned to normal representative stress conditions in 2019. A minor velocity inversion was observed in 2020, and conditions again appeared normal in 2021. These time-lapse observations may reflect periodic failure and associated changes in stress, which currently appears to be stable.

Line 9

Line 9 is a N-S oriented line that runs parallel to Williams Street and crosses wells 52, 53, 59, and 60 at stations 9031, 9061, 9098, and 9127, respectively (Figure 16). Well 60 has had incomplete station coverage in past years due to use of longer receiver spreads but has full coverage with the reduced spread length this year. The overall bulk velocity trend in the shallow portion of the profile observed in 2021 is similar to but slightly higher than the 2020 results. Although the velocity of the upper 30 m has been generally consistent over time, bedrock velocity below 30 m has been variable and elevated with respect to other lines at this site.

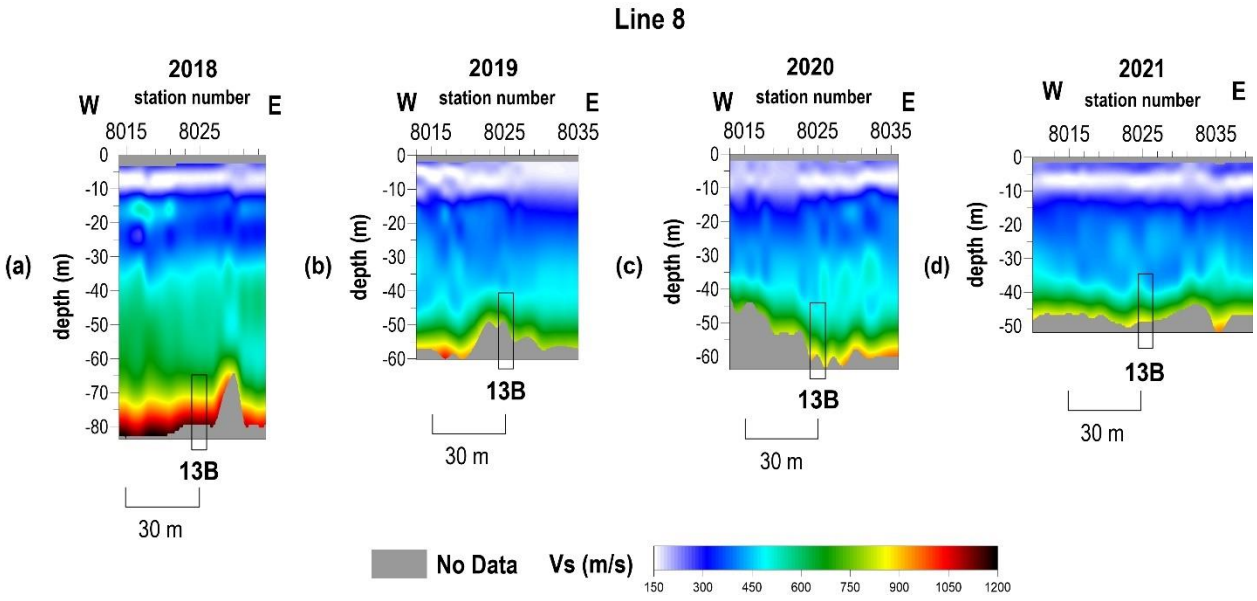

Figure 15. Shear-wave velocity profiles from line 8 from (a) December 2018, (b) December 2019, (c) November 2020, and (d) November 2021.

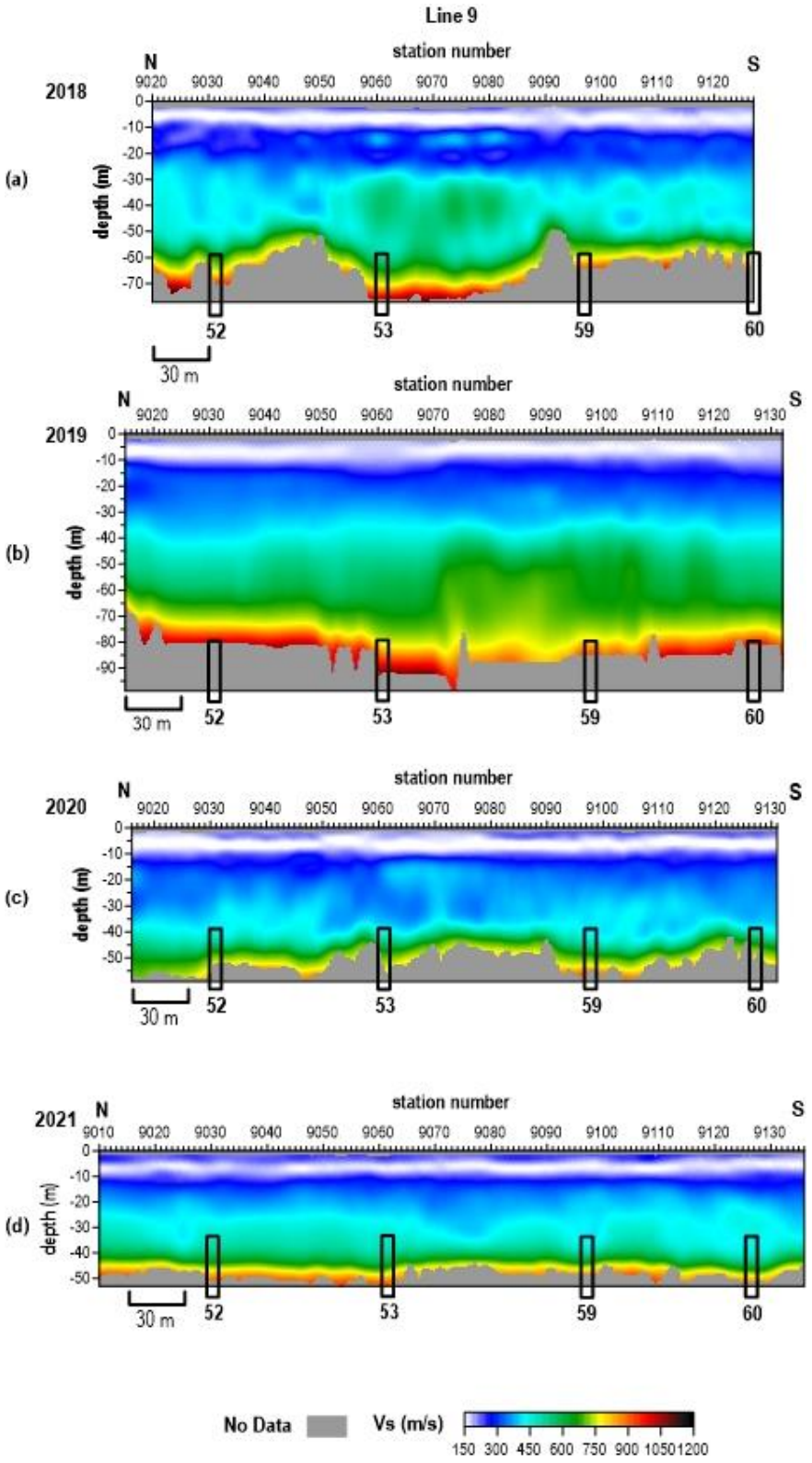

Figure 16. Shear-wave velocity profiles from line 9 from (a) December 2018, (b) December 2019, (c) November 2020, and (d) November 2021.

Line 10

Line 10 is a W-E oriented line that crosses well 2A at station 1022.5 (Figure 17). The westernmost five geophones are located on the road used to access the grain elevator and utilized rock plates instead of steel spikes. Time-lapse changes observed at well 2A since 2013 suggest periods of elevated stress/velocity, subsequent roof rock failure and reduced overburden strength, and periods of relative stability (Appendix, Figure A-1). Between the May 2015 and November 2017 surveys, velocity in the overburden at well 2A increased slightly (~15%) and was consistent with native bedrock velocity. This suggests the void at that time was in a state of relative stability or consumed due to bulking with only gradual changes in stress. Multiple mode behavior was noted west of well 2A in 2020, suggesting heterogeneity at deeper depths where multiple stress states may exist within the shale bedrock. Overall, the bulk velocity trend of the November 2021 result is generally consistent with the 2020 results.

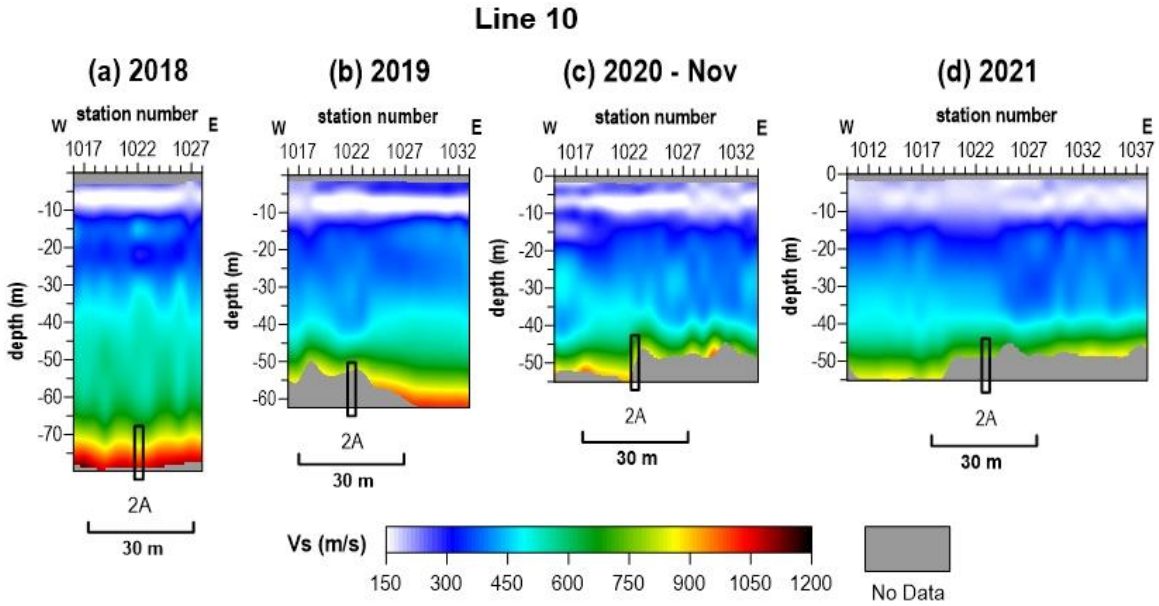

Figure 17. Shear-wave velocity profiles from line 10 from (a) October 2018, (b) December 2019, (c) November 2020, and (d) November 2021.

Line 11

Line 11 is oriented N-S over well 2A at station 1124 and well 4B at station 1151 (Figure 18). High-frequency noise from blower fans in the grain elevator were present on all nights of the survey (Figure 19). Stations with attenuated fundamental mode are coincident with the location of these affected traces, but that is more likely related to lack of coherent source signal since the fans exhibit higher frequency information than the lower frequency range of the missing fundamental mode. The average velocity below 30 m decreased 15% across line 11 from 2019 to 2020. Because such a corresponding decrease was not observed on nearly perpendicular line 10, the velocity variation in 2020 was azimuthal, which is often associated with changes in material strength. In 2021, velocity along this profile increased and nearly returned to 2019 values and appears to be isotropic (consistent with line 10). The time-lapse changes across this line suggest dynamic stress with currently stable conditions.

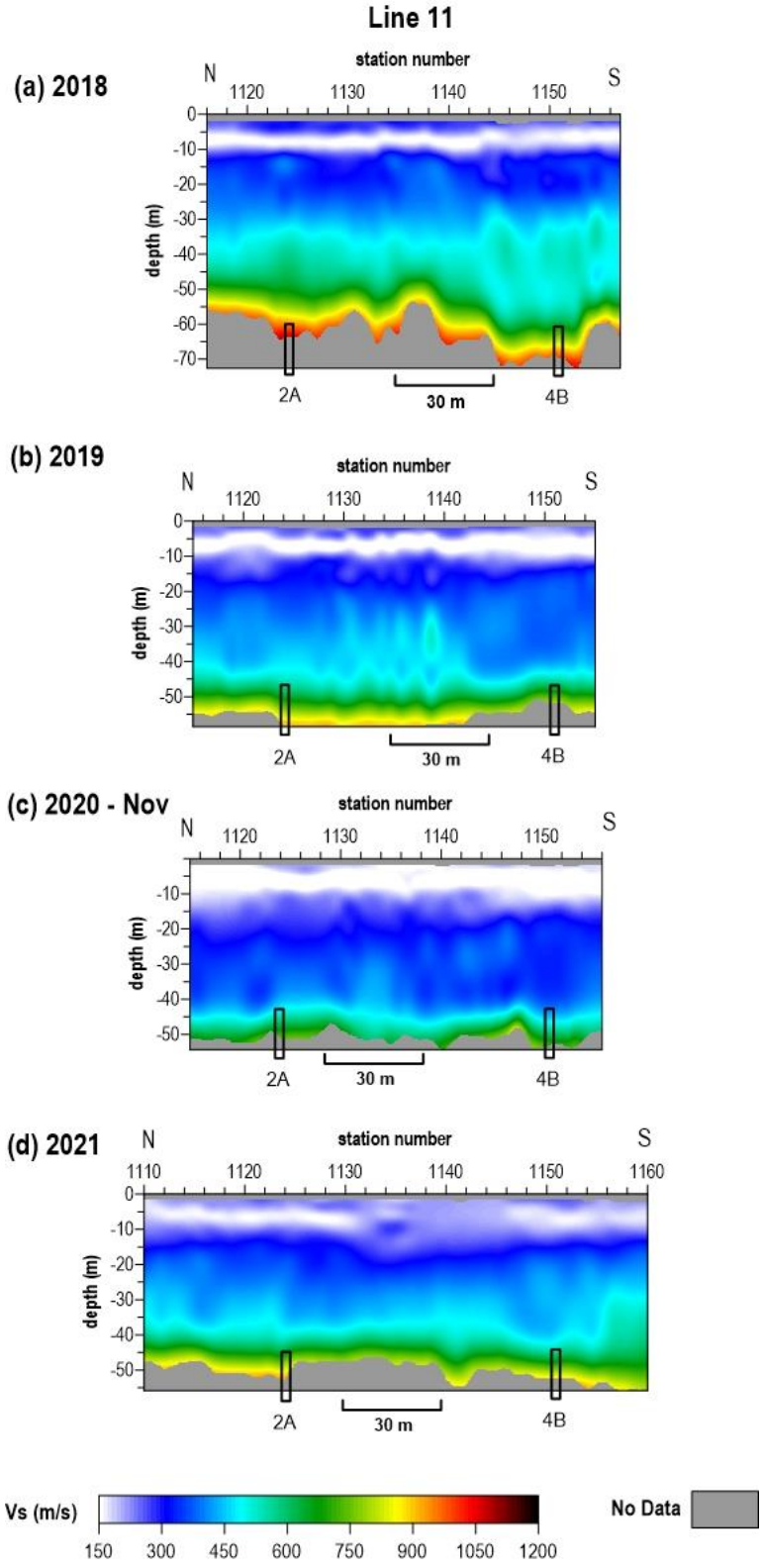

Figure 18. Shear-wave velocity profiles from line 11 from (a) October 2018, (b) December 2019, (c) November 2020, and (d) November 2021.

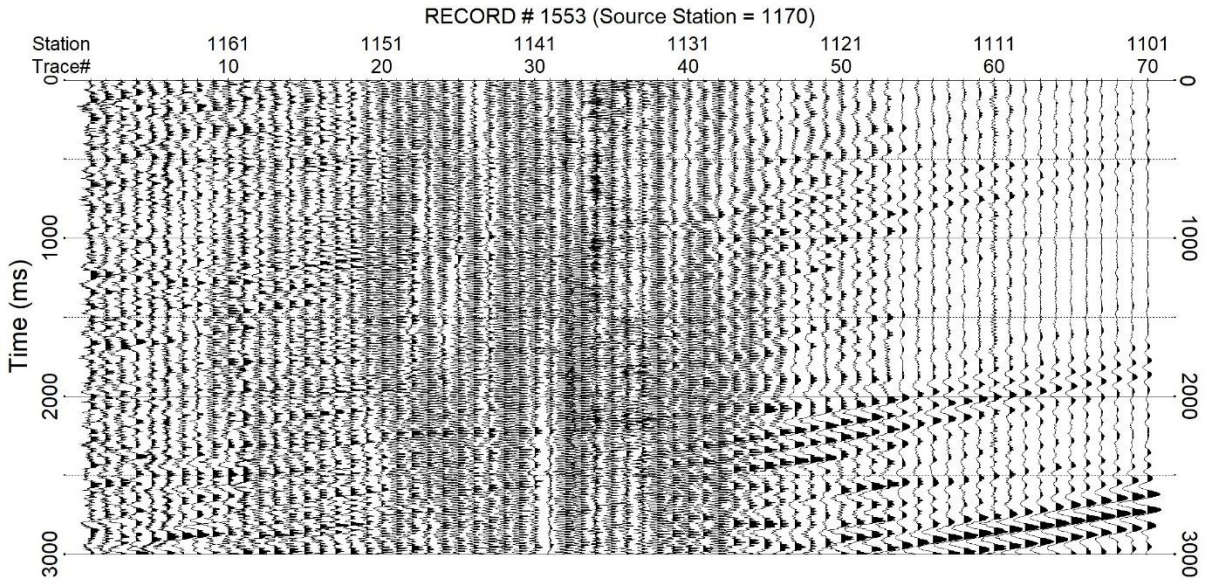

Figure 19. Raw seismic data from line 11. High-frequency noise on traces 19-45 (stations 1152-1126) is attributed to fans running in elevators during acquisition.

Line 12

Line 12 is a W-E oriented line that crosses wells 6B and 7B at stations 1238 and 1219, respectively (Figure 20). An approximately 25% velocity increase was observed in 2020 compared to previous years but was still within the range of bedrock velocity estimates on other lines at the CBRA and may have been a result of higher mode interference with the fundamental mode. Bulk velocity decreased in 2021 and is more consistent with the 2018 and 2019 results, suggesting a normal stress regime.

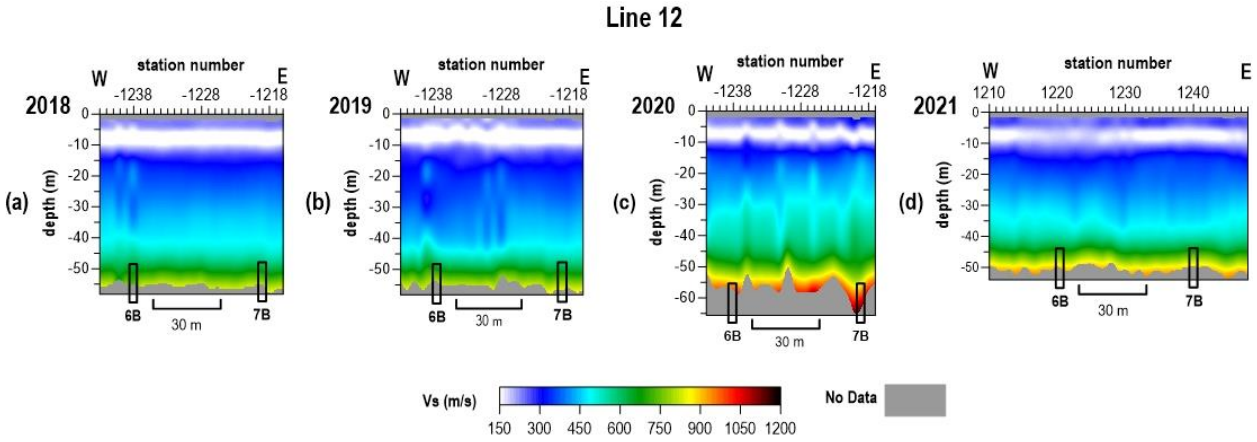

Figure 20. Shear-wave velocity profiles from line 12 from (a) December 2018, (b) December 2019, (c) November 2020, and (d) November 2021.

Line 13

Line 13 is oriented W-E and intersects wells 7A and 4A located approximately at stations 1328 and 1376.5, respectively (Figure 21). The bulk velocity trend has remained relatively consistent since 2018. Although the apparent velocity along line 13 was slightly elevated in 2020, higher than expected velocities were likely the result of higher modes masking the fundamental-mode trend. Velocity values across this area are within normal range for native material and represent a normal stress regime.

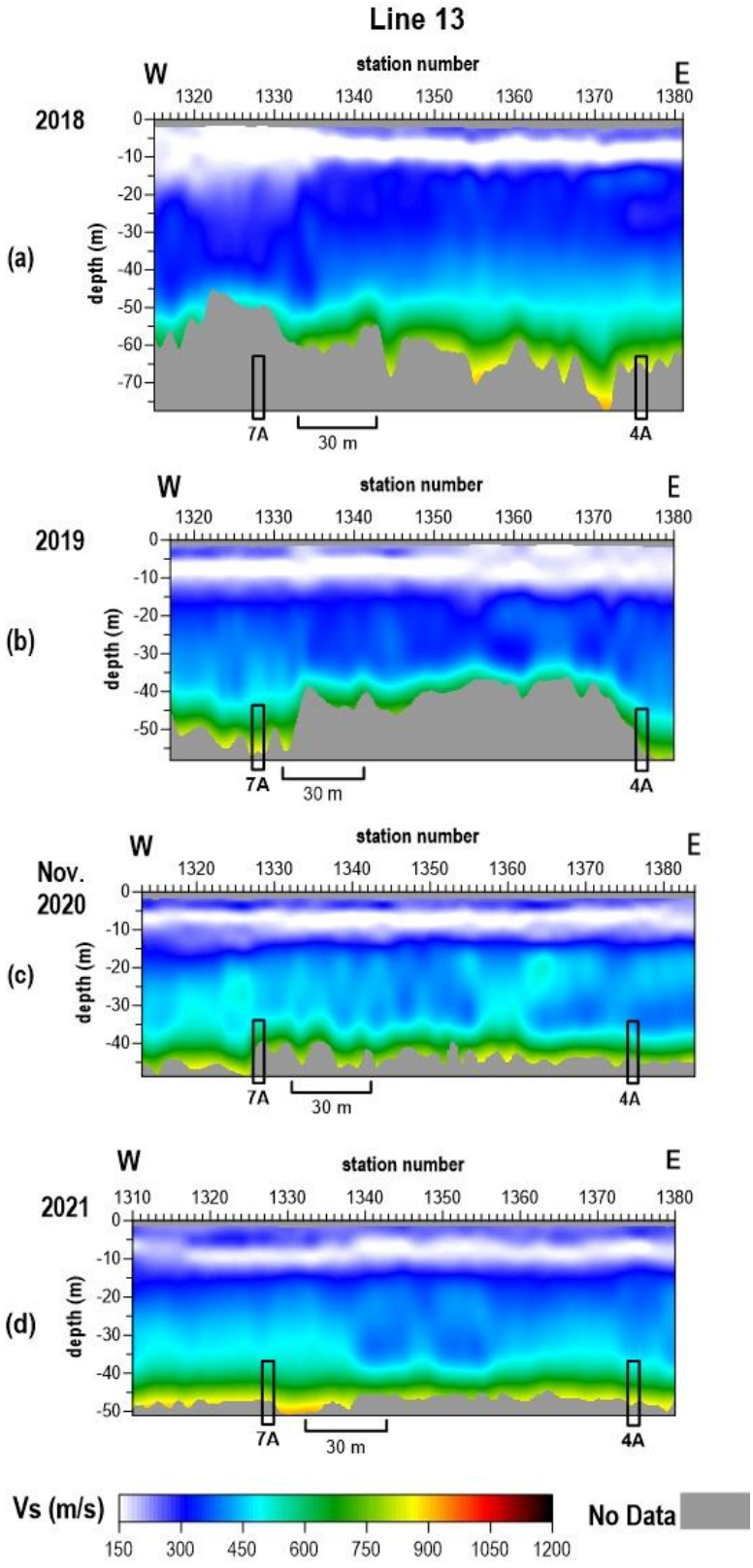

Figure 21. Shear-wave velocity profiles from line 13 from (a) December 2018, (b) December 2019, (c) November 2020, and (d) November 2021.

Line 14

Line 14 is oriented W-E and extends across wells 3B and 1B, which are approximately located at stations 1442 and 1423, respectively (Figure 22). A slight increase in velocity is observed west of well 3B at stations 1410-1425 but is well within the expected bedrock velocity range. A similar increase in velocity has been observed west of this well in past results. Overall bulk velocity profiles suggest a normal stress regime.

Line 15

Line 15 is oriented NW-SE over wells 19, 20, 25, 26, 33, 36, and 94 (Table 5). This line is a new addition to the passive monitoring survey but spans a portion of a 2-D profile recorded during a 2010 passive surface-wave survey. The overall bulk velocity trend for line 15 (Figure 23) is largely consistent with other lines within the CBRA and the 2010 survey (Figure 24). Subtle (~10%) variability in bedrock velocity is observed on the western portion of the line, spanning wells 19, 20, and 25. Relative velocity highs occur at and west of well 19 and at well 20 with relative velocity lows between wells 19 and 20 and between wells 20 and 25. The velocity variability is well within the range expected for natural variation and inherent uncertainty, and with only a single survey it is unclear how it relates to changes in the underlying salt caverns. A collapsed salt jug has a 40 m wide surface expression at and east of well 19. The relative velocity low between wells 19 and 20 could be indicative of reduced bedrock strength associated with the previous well 19 collapse and associated structural feature. Lack of surface expression between wells 20 and 25 suggests the relative velocity at this well could be natural geologic variation or a past failure that has either arrested or not had time to enlarge the roof sufficient to build stress. Aside from these features, the bulk velocity trend suggests an otherwise normal stress regime. Interpretations of wells along this line would benefit greatly from a time-lapse approach to better understand the degree of change to complement current estimated stress.

Table 5. Wells and corresponding station numbers across line 15.

Well	19	20	25	26	33	36	94
Station No.	15025	15058	15080	15123	15138	15174	15207

Dispersion curves for stations around the collapsed salt jug show lower and less coherent fundamental-mode energy compared to stations where the receiver spread was fully away from the feature (Figure 25). Higher mode energy is observed in the overtone image near the collapse feature between 5.5 Hz and 6.5 Hz (Figure 25a). A representative dispersion curve, where the spread is fully outside the surface expression, exhibits a single fundamental-mode trend that is coherent over most frequencies (Figure 25b). This multimode behavior supports the suggestion that multimode dispersion patterns may be an indication of heterogeneities at depth for wells over salt jugs that have not migrated to the surface.

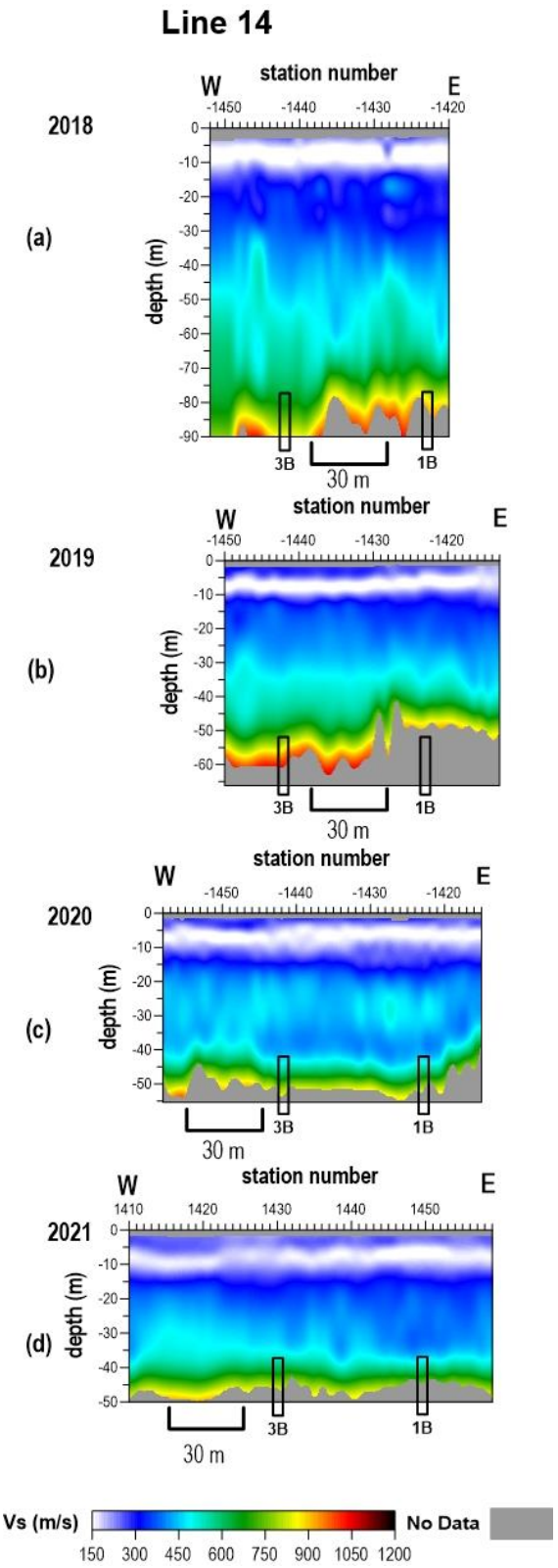

Figure 22. Shear-wave velocity profiles from line 14 from (a) December 2018, (b) December 2019, (c) November 2020, and (d) November 2021.

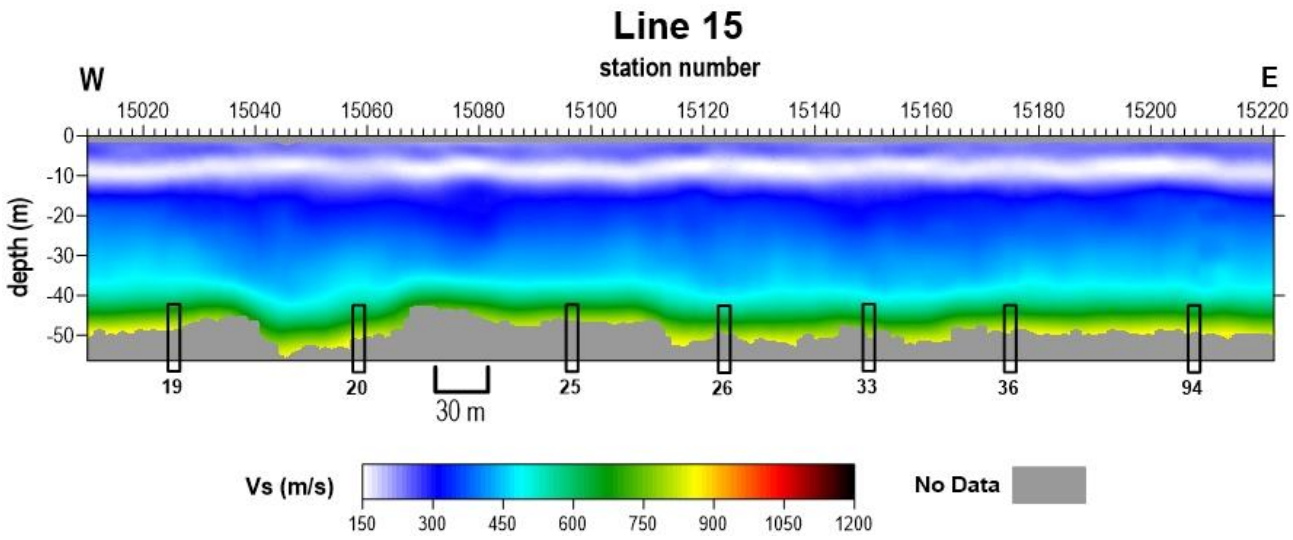

Figure 23. Shear-wave velocity profile from line 15 from the current November 2021 survey.

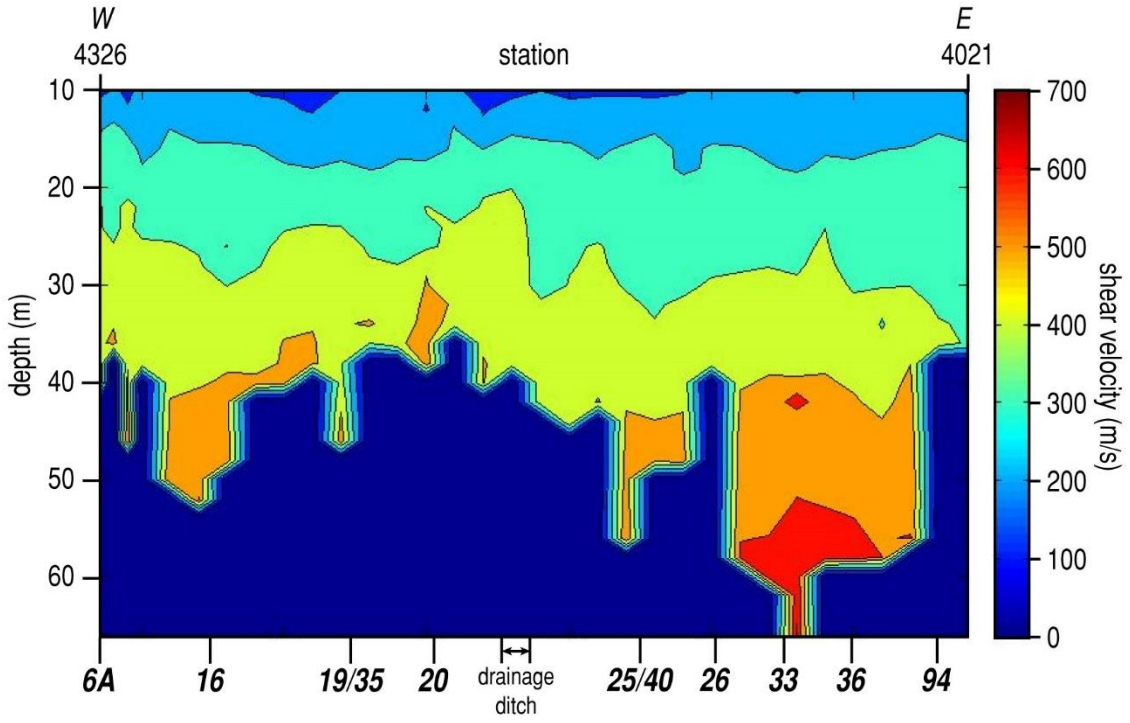

Figure 24. Shear-wave velocity profile from the 2010 survey over the location of line 15 in the current survey.

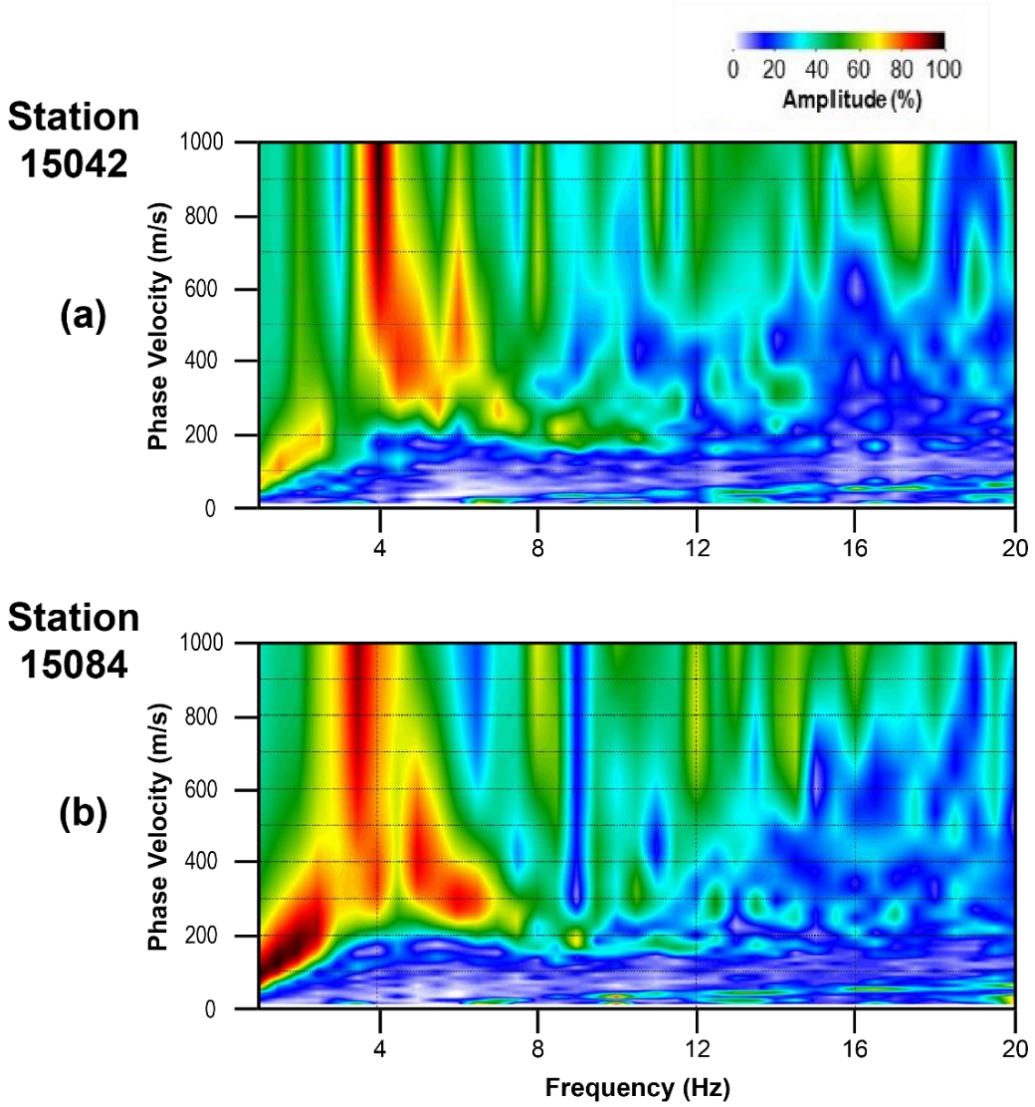

Figure 25. Representative dispersion curves (a) over low velocity anomaly and (b) toward the middle of line 15.

Interpretation and Discussion

A grid of seismic lines is deployed each year with varying lengths and orientations to assess and monitor bedrock conditions around wells of interest within the CBRA. In addition to comprehensive assessment of individual wells (below), analysis and interpretations of these lines were grouped by geographic location on the site to assess site-wide pseudo-3D (2.5-D) velocity trends and identify anomalous features, if any, spanning multiple lines (Appendix, Figures A-2 to A-7). Overall bulk shear-wave velocity trends were consistent between adjacent lines. The only anomalous velocity feature that appears to span multiple adjacent lines is an area with slightly increased velocity south of well 4B on line 11, which appears consistent with a small increase in velocity between wells 4B and 3B on line 14. This may suggest an area of elevated velocity in proximity to the southeast corner of the grain elevator. Because this feature does not appear to be concentrated at a particular well and the velocity in this area has been consistent for the past few years, it most likely represents natural geologic variation, but the potential for this increased velocity (stress) area to be an indicator of an irregular gallery cannot be completely ruled out.

Wells with conditions of normal stress regime and consistent surface-wave behavior

Wells 1B, 6B, 7B, 10B, 11B, 15B, 23, 23B, 25, 26, 29, 30, 33, 36, 39, 41, 42, 44, 46, 87, 88, 89, 90, 92, and 94.

Wells with varied surface-wave behavior but interpreted as consistent with normal or currently stable stress regime

Wells 3B, 4A, 7A, and 8B

Past reports have called out these wells for having attenuated fundamental-mode energy and corresponding limited depth of investigation. Depths across these wells were more consistent with surrounding stations on 2021 data; however, inversion error was larger at stations near these wells. Nonetheless, bulk velocity trends acquired over these wells likely represent natural geologic conditions with a normal stress regime.

Wells 13B and 15B

Velocity at well 13B was elevated in 2018, reduced to expected bedrock velocity in 2019, and slightly elevated in 2020. Elevated velocity at depth and associated increase in depth of investigation near well 15B prompted a midyear monitoring survey in August 2020. Time-lapse observations suggest dynamic changes at these wells that could be related to variations in roof rock properties; however, subsurface conditions at the time of the 2021 survey appear stable.

Wells 52, 53, 59, 60 (Williams Street)

The velocity gradient in the upper 30 m of the Williams Street line (line 9) has been reasonably consistent since the beginning of time-lapse passive surface-wave monitoring. Velocity trends below 30 m have varied slightly over time and are typically elevated compared to other lines at the CBRA. Either shear stress or bedrock velocity appears to be higher along this line. Currently, there are no anomalies observed in the velocity profile that would suggest vertical void migration is imminent at any of the wells on this line.

Wells 2A and 4B

Well 2A is intersected by lines 10 and 11. Multimode dispersion curves have been observed near well 2A along line 10, potentially indicative of heterogeneity below the imaging depth of these data. Well 4B is intersected by lines 5 and 11. In 2020, azimuthal variation in bedrock velocity was noted between lines 10 and 11 with a relative 15% decrease in velocity on line 11. In 2021, the estimated shear-velocity trend increased with a velocity profile that is more consistent with lines 10 and 5. The timelapse changes across this line suggest dynamic stress changes with data from the 2021 survey indicative of a period with stable conditions.

Wells with possibly varying stress regime

Wells 17, 22A, 42, and 45

An area of elevated velocity was observed between wells 17 and 42 (line 1) and 45 and 22A (line 3) in 2020. This year, the overall velocity trend is more consistent with the 2019 result with a more uniform profile between wells on lines 1 and 3 with only subtle velocity hallows near wells 17 and 42. This kind of observation is consistent with the dynamics of this site and these wells.

Wells 2B, 12B, and 14B

A subtle halo anomaly was observed between wells 2B and 12B on line 5 in 2020. In 2021, the velocity profile between these wells returned to baseline bedrock velocity, indicative of normal geologic variation. However, just east of well 12B, a dome-shaped area of elevated velocity has appeared near well 14B. Time-lapse observations along line 5 over the past few years suggest that dynamic stress changes are occurring and that they are possibly associated with changes in the roof structures/characteristics of salt jugs at these three wells.

Well 8A

The halo anomaly observed over well 8A in 2018 and 2020 persists in 2021. The relative magnitude, depth, and shape of this anomaly has remained consistent throughout this time. The velocity is within the bounds of native material, but due to its apparent absence in 2019, it may be an indicator of dynamic processes at depth and currently elevated stress in the bedrock overlying well 8A.

Wells 19, 20, and 25

Lower velocities were observed near wells surrounding a sinkhole along line 15. Dispersion curves around this collapse feature exhibit multiple modes across lower frequencies and an overall decrease in the fundamental-mode phase velocity. Since this is the first year wells 19 and 20 were included in the study, no determinations can be made at this time of the existence of a dynamic stress regime.

Conclusions and Recommendations

The shear-wave velocity directly over or in proximity to a majority of the wells in this 2021 study continues to represent natural geologic conditions and a normal stress regime. Shear-wave velocity profiles were classified into three categories based on measurements and wave observations in overburden above and in proximity to each well. They are 1) normal stress regime and well-behaved surface-wave propagation, 2) inconsistent surface-wave behavior and normal or currently stable stress regime, and 3) changes in stress regime. Anomalous shear-wave velocity profiles from seven wells are sufficiently outside the normal range to justify a heightened awareness and focused monitoring on future surveys.

Strength characteristics estimated from shear-wave velocities that were derived from the passive MASW surveys around wells 8A, 17, 42 (line 1), 14B (line 5), 19, 20, and 25 (line 15) have changed from historical surveys and are consistent with possible increases in stress due to under-supported spans of roof rock above voids. Voids associated with these seven wells currently represent the only apparent potential threat to ground stability in the survey area. However, it should be noted that the Williams Street line (line 9 spanning wells 52, 53, 59, and 60) has overall higher bedrock velocity below 30 m compared to other lines at the CBRA, and higher stress is generally a precursor to failure. A history of elevated stress/velocity at depth and dynamic stress/velocity measurements have been observed at wells 2A and 4B (and, while currently normal or stable, were the focus of considerable concern and discussion in past reports). In general, since current conditions largely reflect normal or stable stress regimes with a few areas possessing subtle and relatively minimally elevated stress, we recommend continued monitoring on an annual basis with no apparent need this year for a well-specific interim survey.

References

Davies, W.E., 1951, Mechanics of Cavern Breakdown. Bulletin of the National Speleological Society, no. 13, 36-43.

Dellwig, L.F., 1963, Environment and mechanics of deposition of the Permian Hutchinson Salt Member of the Wellington shale: Symposium on Salt, Northern Ohio Geological Society, p. 74-85.

Dvorkin, J., A. Nur, and C. Chaika, 1996, Stress sensitivity of sandstones: *Geophysics*, v. 61, p. 444-455.

Eberhart-Phillips, D., D.-H. Han, and M.D. Zoback, 1989, Empirical relationships among seismic velocity, effective pressure, porosity, and clay content in sandstone: *Geophysics*, v. 54, p. 82-89.

Holdoway, K.A., 1978, Deposition of evaporites and red beds of the Nippewalla Group, Permian, western Kansas: Kansas Geological Survey Bulletin 215.

Ivanov, J., R.D. Miller, S.L. Peterie, J.T. Schwenk, J.J. Nolan, B. Bennett, B. Wedel, J. Anderson, J. Chandler, and S. Green, 2013, Enhanced passive seismic characterization of high priority salt jugs in Hutchinson, Kansas: Preliminary report to Burns & McDonnell Engineering Company.

Khaksar, A., C.M. Griffiths, and C. McCann, 1999, Compressional- and shear-wave velocities as a function of confining stress in dry sandstones: *Geophysical Prospecting*, v. 47, p. 487-508.

Kulstad, R.O., 1959, Thickness and salt percentage of the Hutchinson salt; *in* Symposium on Geophysics in Kansas: Kansas Geological Survey Bulletin 137, p. 241-247.

McGuire, D., and B. Miller, 1989, The utility of single-point seismic data; *in* Geophysics in Kansas, D.W. Steeples, ed.: Kansas Geological Survey Bulletin 226, p. 1-8.

Merriam, D.F., 1963, The Geologic History of Kansas: Kansas Geological Survey Bulletin 162, 317 p.

Merriam, D.F., and C.J. Mann, 1957, Sinkholes and related geologic features in Kansas: *Transactions of the Kansas Academy of Science*, v. 60, p. 207-243.

Miller, R.D., 2011, Progress report: 3-D passive surface-wave investigation of solution mining voids in Hutchinson, Kansas: Interim report to Burns & McDonnell Engineering Company, January, 9 p.

Miller, R.D., J. Ivanov, S.D. Sloan, S.L. Walters, B. Leitner, A. Rech, B.A. Wedel, A.R. Wedel, J.M. Anderson, O.M. Metheny, and J.C. Schwarzer, 2009, Shear-wave study above Vigindustries, Inc. legacy salt jugs in Hutchinson, Kansas: Kansas Geological Survey Open-file Report 2009-3.

Morton, S.L., J. Ivanov, S. Peterie, R. Miller, B. Bennett, C. Gonzalez, E. Knippel, C. Umbrell, and B. Wedel, 2021, Passive seismic characterization of high priority salt jugs near Hutchinson, Kansas: November 2020: Kansas Geological Survey Open-file Report 2021-10, 70 p.

Morton, S.L., R.D. Miller, J. Ivanov, S.L. Peterie, and, R.L. Parsons, 2020a, Time-lapse monitoring of stress-field variations within the Lower Permian shales in Kansas: *The Leading Edge*, 39, no. 5,318-323. doi: 10.1190/tle39050318.1.

Morton, S.L., S. Peterie, J. Ivanov, R. Miller, B. Bennett, C. Bunker, K. Burke, E. Knippel, J. Lawler, C. Umbrell, and B. Wedel, 2020b, Passive seismic characterization of high priority salt jugs near Hutchinson, Kansas: December 2019: Kansas Geological Survey Open-file Report 2020-15, 39 p.

Park, C., R. Miller, D. Laflen, N. Cabrillo, J. Ivanov, B. Bennett, and R. Huggins, 2004, Imaging dispersion curves of passive surface waves [Exp. Abs.]: Annual Meeting of the Soc. of Expl. Geophys., Denver, Colorado, October 10-15, p. 1357-1360.

Sayers, C.M., 2004, Monitoring production-induced stress changes using seismic waves [Exp. Abs.]: Annual Meeting of the Soc. of Expl. Geophys., Denver, Colorado, October 10-15, p. 2287-2290.

Sloan, S.D., R.D. Miller, J. Ivanov, and, S. Walters, 2009, Shear-wave velocity as an indicator of increased stress and failure potential associated with dissolution mining voids: Symposium on the Application of Geophysics to Engineering and Environmental Problems, 363-372. https://doi.org/10.4133/1.3176713.

Sloan, S.D., S.L. Peterie, J. Ivanov, R.D. Miller, and J.R. McKenna, 2010, Void detection using near-surface seismic methods; *in* Advances in Near-Surface Seismology and Ground-Penetrating Radar, SEG Geophysical Developments Series No. 15, R.D. Miller, J.D. Bradford, and K. Holliger, eds.: Tulsa, Society of Exploration Geophysicists, p. 201-218.

Swineford, A., 1955, Petrography of upper Permian rocks in south-central Kansas: State Geological Survey of Kansas Bulletin 111, 179 p.
Walters, R.F., 1978, Land subsidence in central Kansas related to salt dissolution: Kansas Geological Survey Bulletin 214, 82 p.
Whittemore, D.O., 1990, Geochemical identification of saltwater contamination at the Siefkes subsidence site: Report for the Kansas Corporation Commission.
Whittemore, D.O., 1989, Geochemical characterization of saltwater contamination in the Macksville sink and adjacent aquifer: Kansas Geological Survey Open-file Report 89-35.

Appendix

Line 10 Previous Results

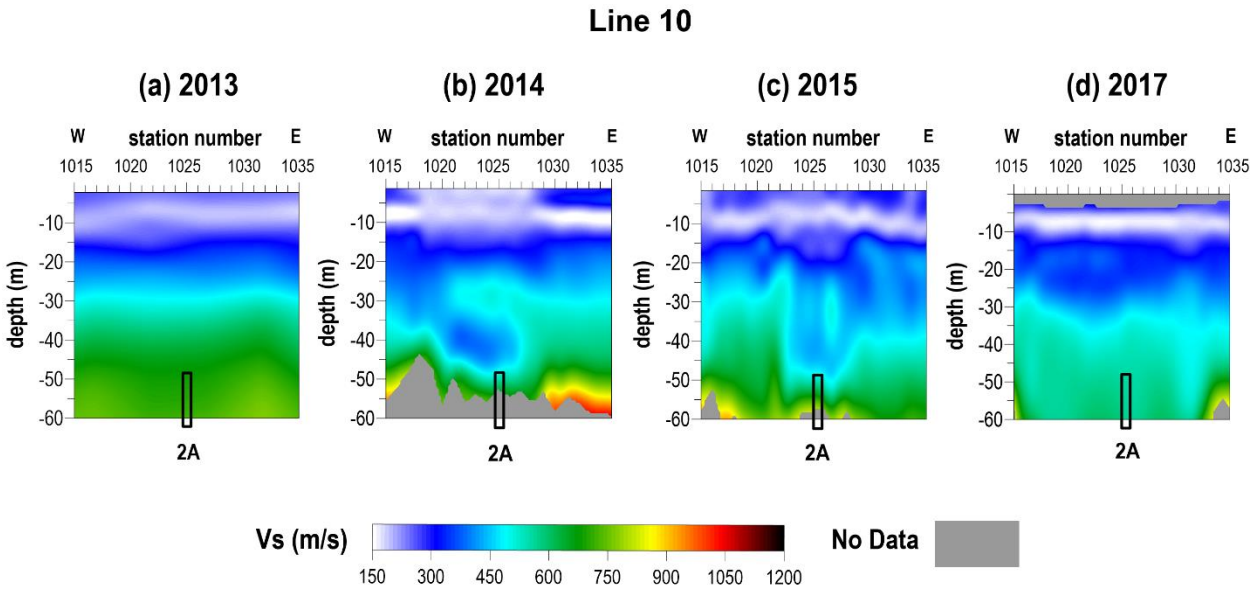

Figure A-1. Shear-wave velocity profiles for line 10 over well 2A for years 2013-2017.

2.5D Interpretation

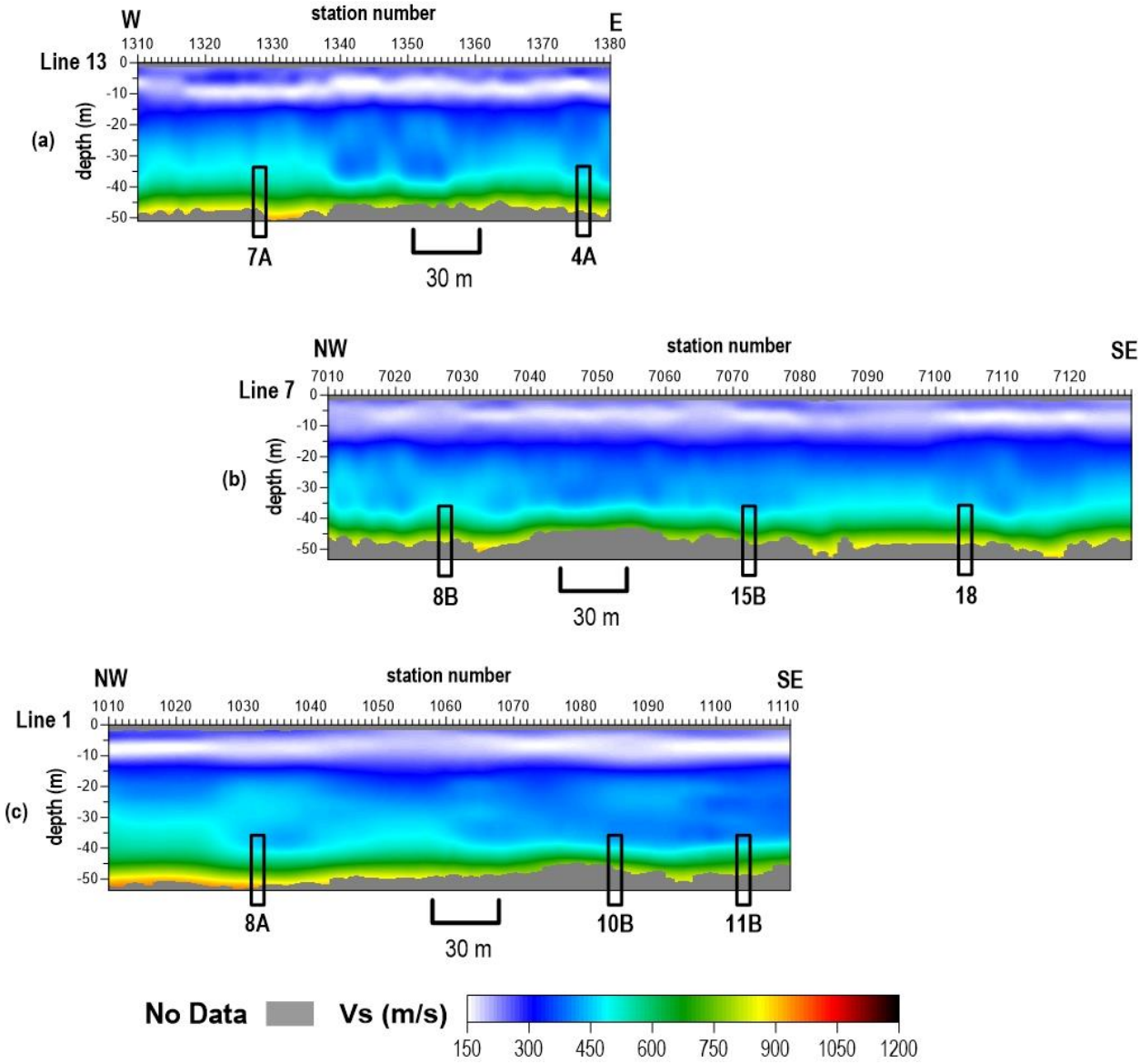

Figure A-2. Shear-wave velocity profiles from (a) line 13, (b) line 7, and (c) line 1 of the current investigation.

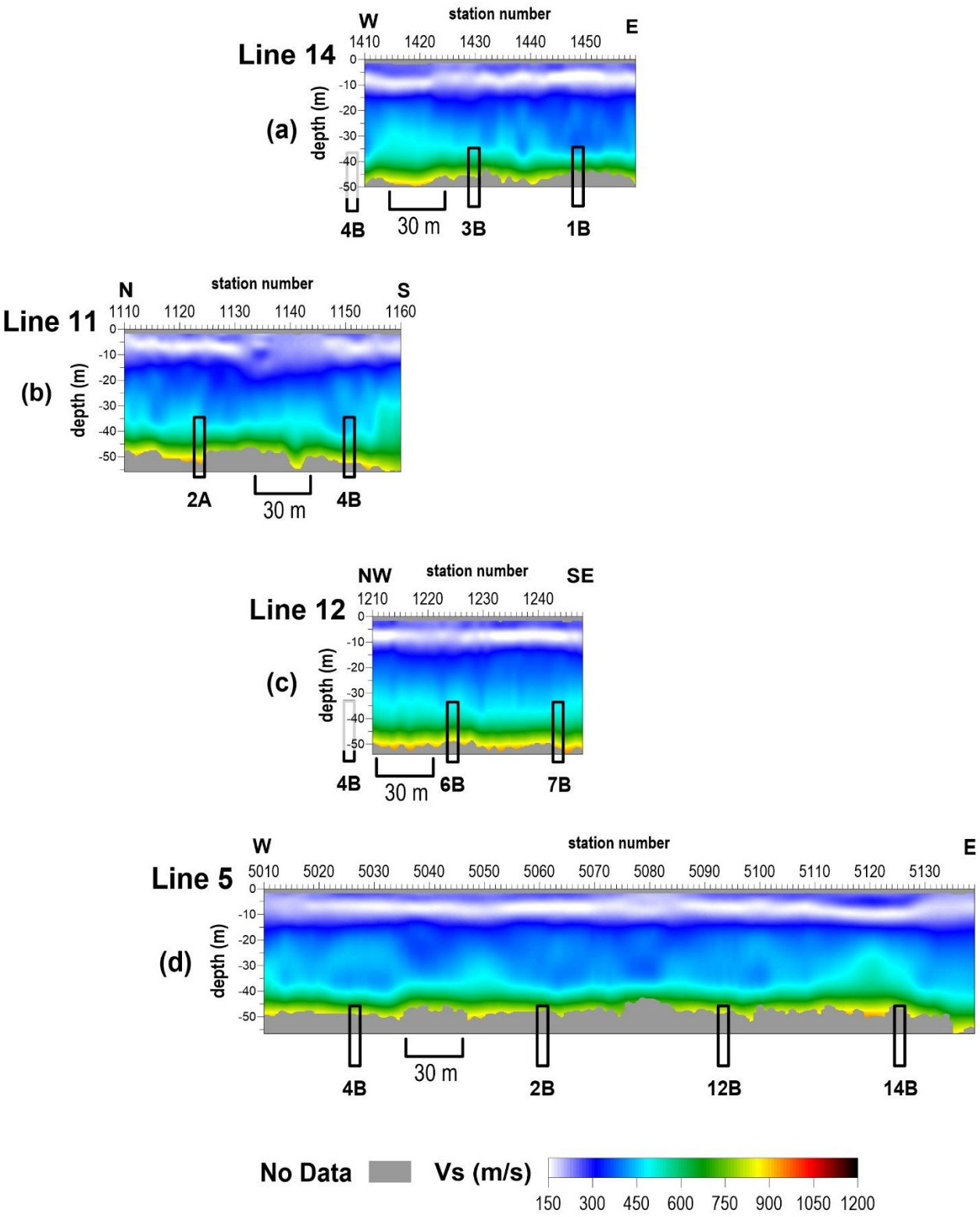

Figure A-3. Shear-wave velocity profiles from (a) line 14, (b) line 11, (c) line 12, and (d) line 5 of the current investigation.

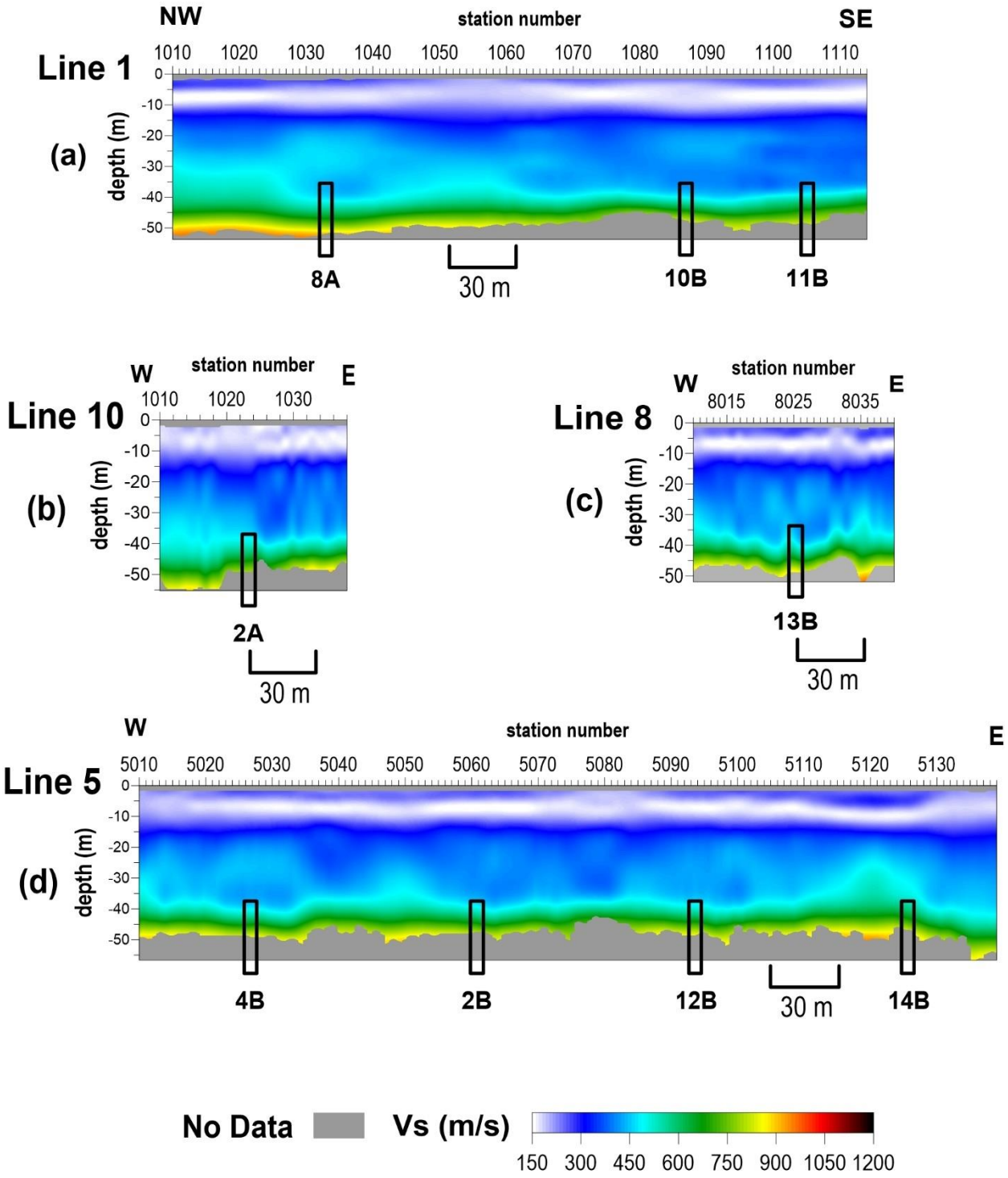

Figure A-4. Shear-wave velocity profiles from (a) line 1, (b) line 10, (c) line 8, and (d) line 5 of the current investigation.

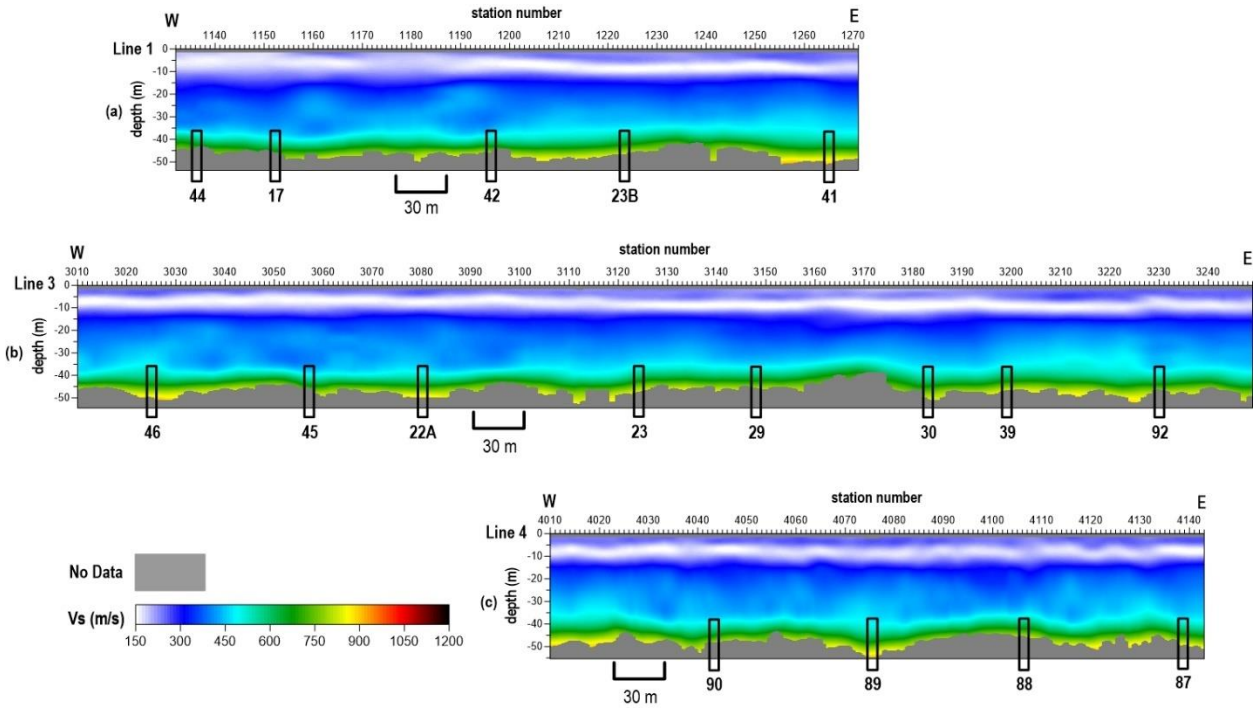

Figure A-5. Shear-wave velocity profiles from (a) line 1, (b) line 3, and (c) line 4 of the current investigation.

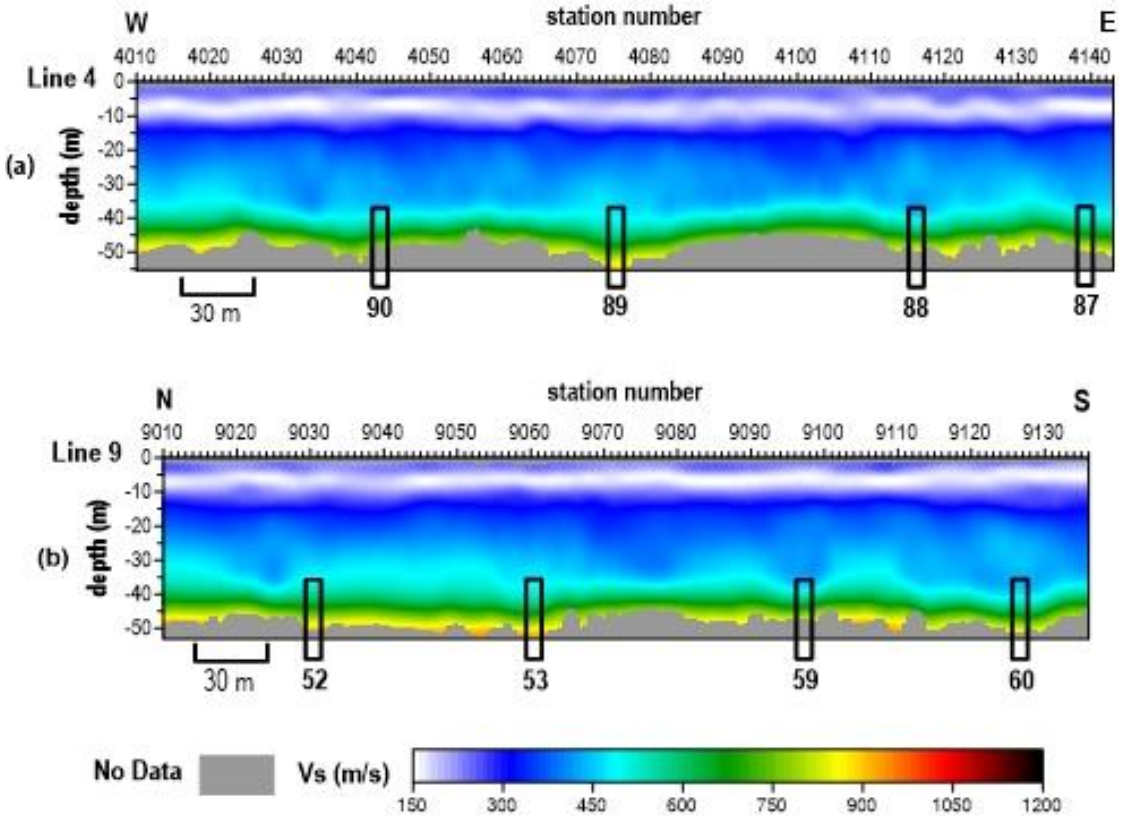

Figure A-6. Shear-wave velocity profiles from (a) line 4 and (b) line 9 of the current investigation.

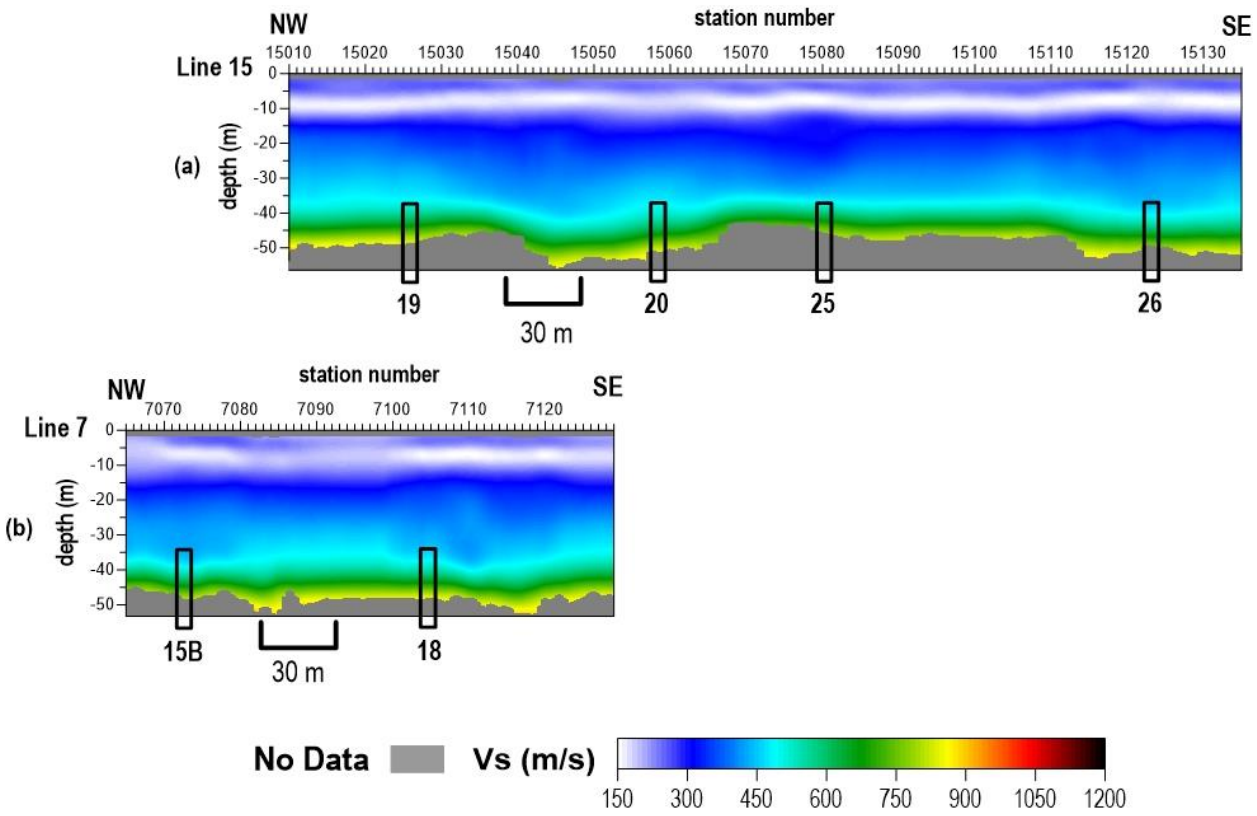

Figure A-7. Shear-wave velocity profiles from (a) line 15 and (b) line 7 of the current investigation.